



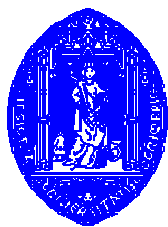
**Departamento de Física
da Universidade de Coimbra**

Laser Doppler Flowmetry

Project Report
5th year
Graduation in Biomedical Engineering

Ana Isabel Leitão Ferreira

September 2007



Faculdade de Ciências e Tecnologia
da Universidade de Coimbra



Faculdade de Medicina
da Universidade de Coimbra

This report is made fulfilling the requirements of **Project**, a discipline of the 5th year of the Biomedical Engineering graduation course.

Supervisors

Prof. Carlos M. Correia and Prof.
Luís Requiça Ferreira
Physics Department FCTUC



External Supervisor

João Maldonado, MD
Instituto de Investigação e Formação
Cardiovascular



Contents

Acknowledgments	i
Abstract	ii
Sumário	iii
1. Introduction	1
1.1. Motivation	1
1.2. Purpose	2
2. Theoretical Background	3
2.1. Optical properties of tissue	3
2.2. The appropriate wavelength	6
2.3. The Doppler principle for light-scattering	6
2.4. Frequency beating	7
2.5. Detection	9
2.5.1. Homodyne	9
2.5.2. Heterodyne	10
2.6. Light Transportation	11
2.6.1. Free space	11
2.6.2. Fibers	12
2.7. Output	14
2.7.1. Laser Doppler Flowmetry	14
2.7.2. Laser Doppler Imaging	15
2.8. Self-mixing	16
2.8.1. Theory of self-mixing interferometry	16
3. State of the art	19
3.1. Laser Doppler Flowmetry (LDF)	19
3.1.1. Units	20
3.1.2. Applications	20
3.2. Literature	21
3.3. Commercial instruments	22
4. Self-Mixing	25
5. Experimental Setup/Bench Tests	26

5.1. Schedule.....	26
5.2. System Architecture.....	27
5.2.1. Measurement probe.....	28
5.2.2. Interface system	29
5.2.3. Data acquisition and signal processing	33
5.3. Bench Test I.....	35
5.4. Bench Test II.....	36
6. Results.....	38
6.1. Dimensioning.....	38
6.2. Functional Tests	40
6.2.1. Bench Test I	40
6.3. Another Bench Tests.....	42
7. Conclusions and Future Work	44
8. References.....	46
Annexes	
A – Simulation of the beating frequency phenomenon.....	49
B – Specifications Table of DTI OxyLab LDF and OxyFlo.....	50
C – Schematics	
C ₁ – Collimation Tube.....	51
C ₂ – Focusing Tube.....	52
C ₃ – Style a Strain Relief.....	53
D – PCB design.....	54
E – Schematic of the Laser Driver.....	55
F - Specifications of the Low-Cost Multifunction DAQ for USB.....	56
G – Matlab routines to observe LDF data acquisition.....	57

Table of Figures

Figure 1: Structure of the skin, illustrating the blood vessels.....	4
Figure 2: Absorption spectra for HbO ₂ and HbO.	5
Figure 3: The principle of LDF.....	7
Figure 4: Beating phenomenon of two frequencies F1 and F2.	9
Figure 6: Schematic diagram of laser Doppler in free space using fiber optic cable.....	12
Figure 7: Blood perfusion monitoring	13
Figure 8: Signals of LDF output	14
Figure 9: Schematic of LDI	15
Figure 10: Blood flow-related images of human fingers	15
Figure 11: Three-mirror cavity model used to analyze the optical feedback configuration.	17
Figure 12: Basic principle of LDF	19
Figure 13: Commercial instruments used to measure LDF	23
Figure 14: Example of DTI Oxylab output.....	23
Figure 15: My schedule diagram.	26
Figure 16: Block diagram of the complete system.	27
Figure 17: Prototypes 1 (top) and 2 (bottom).	28
Figure 18: Schematic of the dual polarity current source.	30
Figure 19: Schematic of the transconductance amplifier used in laser driver circuit.	31
Figure 20: Schematic of the voltage follower.....	31
Figure 22: Schematic of the DC-DC Converter.....	32
Figure 23: NI USB-6009.....	32
Figure 21: Schematic of the audible monitoring.....	32
Figure 24: Flowchart of the Matlab programmer.	34
Figure 25: Image of the experimental arrangement I for LDF detection.....	35
Figure 26: Image of the experimental arrangement II for LDF detection.....	37
Figure 27: The loudspeaker arrangement.	38
Figure 28: The moving strip arrangement.	39
Figure 29: Typical signals observed in self-mixing.....	40
Figure 30: Frequency Beating Spectra.....	41
Figure 31: Hydraulic Model. The solution enters to the tube and flows through it.....	42

Acknowledgments

I would like to thank to Professors Carlos Correia and Requicha Ferreira, my supervisors and main responsible for the accomplishment of the project, for their contribution, support, excused attention and patience. I appreciate all the chances of opening doors for the success of this project: methodologies and tools of my work.

I would like to thank to Dr. João Maldonado, my external supervisor, for the project idea and for the offered possibility of partial accomplishment of this project in the Instituto de Investigação e Formação Cardiovascular de Coimbra (IIFC).

I would like to thank to the Faculdade de Ciências e Tecnologia de Coimbra, for the formation given throughout these years, particularly to professors such as Doctor Miguel Morgado who marked our way of thinking and acting.

I would like to thank to the elements of the Grupo de Electrónica e Instrumentação that have received and followed us with gentleness, for all the availability, understanding and confidence that had deposited in us.

I am thankful to Eng. Augusto for his help concerning the metallic parts machined.

I am thankful to Edite and Catarina, my daily partners of work, for the conviviality and availability in helping when even it was required.

I am thankful to Hugo Natal da Luz, for the reviewing of my report.

Finally, and not less important, I would like to give thanks to my friends who have been always by my side and to my family, that have supported me financially and affectively, and always trusted my capacities through all these years.

Abstract

This report describes the work developed in the discipline Project of the 5th year of Biomedical Engineering graduation course at the University of Coimbra.

This work, entitled “Evaluation of Hemodynamic parameters: Laser Doppler Flowmetry”, has as final goal, the development of hardware and software solutions capable of being integrated in instruments for measuring blood perfusion using the optical laser Doppler technique.

In the first part of this report, the theoretical and functional principles are reviewed and discussed. They are extremely important to the full understanding of the second part of this study, namely the construction of experimental set-ups that aim at testing some implementations of the self-mixing technique for LDF. Two arrangements were made, one that uses a loudspeaker and another with a moving strip arrangement. Software routines to assess these implementations are also discussed.

Other bench tests are only suggested, due to the lack of time required to its full exploitation.

Sumário

O presente relatório visa fazer uma exposição do trabalho elaborado no âmbito da disciplina de Projecto do 5º ano da Licenciatura em Engenharia Biomédica da Universidade de Coimbra.

Este trabalho, intitulado “Avaliação de Parâmetros Hemodinâmicos: Laser Doppler Pontual”, tem como objectivo, o desenvolvimento de hardware e software capaz de ser integrado em instrumentos para medição de perfusão sanguínea usando a técnica de laser Doppler.

Na primeira parte do relatório revêm-se e discutem-se os princípios teóricos e de funcionamento da técnica. Estes são extremamente importantes para a compreensão da segunda parte deste relatório, mais precisamente na construção de experiências que pretendem testar algumas implementações da técnica de self-mixing no LDF. Foram desenvolvidas duas experiências de bancada, uma que usa um altifalante e outra relacionada com uma tira de papel móvel. Também são discutidas rotinas de software para estas aplicações.

Numa última parte, são apenas sugeridas outras experiências de bancada que requerem futuras explorações.

1. Introduction

In this section, the motivation and objectives of this work will be outlined.

1.1. Motivation

One of the most interesting parameters of Hemodynamic evaluation is the quality of arterial microcirculation. Study and knowledge in this area is, nowadays, one of the most important goals not only for cardiologists, but also for all the medical community that have it as an indicator of the general condition of circulatory system and as a diagnostic tool for some pathologies.

The arterial hypertension is characterized by the capillary vessels loss which increases the arterial pressure. As the capillaries of microcirculation are responsible for the irrigation of important organs, the disappearance of these vessels could result in deep diseases associated to arterial hypertension, such as cerebral hemorrhage or myocardial infarction.

Among the few diagnostic techniques available, Laser Doppler Flowmetry (LDF) introduced by Stern in 1975 has been the one that has the greatest developments either in the medical perspective or in the possibility that new instrumental device integration confers to the measurement system. LDF is probably the first truly non-invasive technique for blood perfusion monitoring and it uses the Doppler shifted light as a carrier of information.

However, an important open issue remains, the results are generally expressed in arbitrary units, since there is no agreement on the units for blood perfusion assessment, both in literature and commercial instruments.

1.2. Purpose

This project, in the framework of the discipline of the 5th year of the Biomedical Engineering graduation course it is about arterial hypertension, since that's an extremely important area and where all the human and material resources, nowadays available, allow us to develop techniques and methodologies with a large potential of application. So, we aim at developing instrumental methods to measure blood perfusion in arterial microcirculation and to improve informatic applications that can be used as a graphic interface and as a results interpretation tool.

The instrumental prototypes and the software applications should be suitable to be operated by specialized staff in clinics and hospitals and, in the limit, for clinical use.

2. Theoretical Background

In this chapter, theoretical and functional overviews will be made. The optical properties in the human tissue, the Doppler principle for light scattering, the detection, the light transportation and the output will be described. The appropriate wavelength, the frequency beating and the self-mixing technique will also be depicted.

2.1. Optical properties of tissue

When light interacts with human tissue, it is either absorbed or scattered in different amounts depending on its optical properties. The tissue properties are important for all kinds of laser applications, in order to understand the interaction mechanisms between light and tissue.

Biological materials are very complex and the details of the optical structure of tissue are not completely known. However, thanks to the results of experiments and the theoretical models which have been proposed, a general understanding of the optical behavior of skin has been formulated. The basic anatomy of the skin with the blood vessels is illustrated in figure 1.

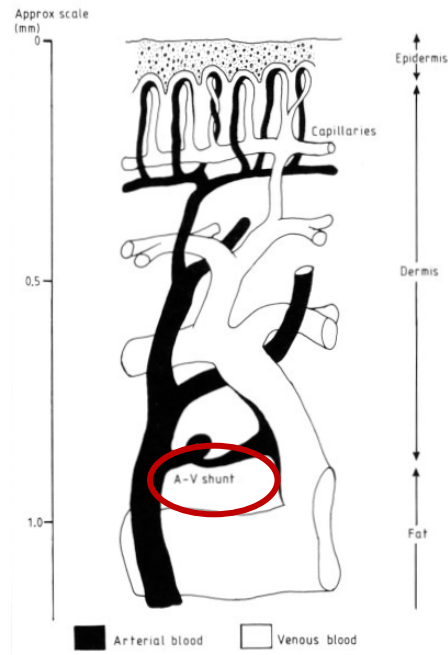


Figure 1: Structure of the skin, illustrating the blood vessels. (Adapted from ^[1])

The diagram is representative but there are considerable variations from one body site to another. The epidermis contains no blood vessels and the dead cells are continually being shed from its surface. However, the dermis contains an extensive set of arterioles, capillaries and venules. The capillaries are about 0.3mm long and 10 μ m in diameter, at a density of 10mm⁻². The capillaries transport the nutrients to the junction between the dermis and epidermis, where cells regeneration takes place. The wall of the capillary is in fact the site of nutrient and waste exchange. They are usually oriented perpendicular to the surface, however, in the skin surrounding the nails, the nail fold, the capillaries are oriented parallel to the surface and they are visible with low-power microscopy ^[1].

Measurement of the blood flow in the skin is not easy by the fact that skin plays an important role in thermoregulation because of the short muscular direct artery-to-vein links, the A-V shunts (see figure 1, red oval line). They are found principally in the toes, fingers, palms and feet. These short blood vessels are closed in the resting state but they can open in response to a thermal stimulus and give as much as a hundredfold increase in blood flow. In addition, the blood vessels calibre can change with emotional state. In the epidermis, melanin is the pigment that determines the majority of absorption in the

visible and in the near-infrared regions. This absorption increases rapidly as the wavelength decreases to protect the skin against ultraviolet radiations. In the epidermis the light scattering is weak but in the dermis scattering from the fibrous tissue is a significant factor in determination of the depth penetration of radiation. Absorption in the vascular dermis is determined by the pigments such the haemoglobin (Hb) contained in the red blood vessels (RBCS). Hemoglobin combines with oxygen in the lungs to form oxyhaemoglobin (HbO₂) that transports the oxygen through the body.

The absorption spectrum of hemoglobin and oxyhaemoglobin in the visible region is illustrated in figure 2.

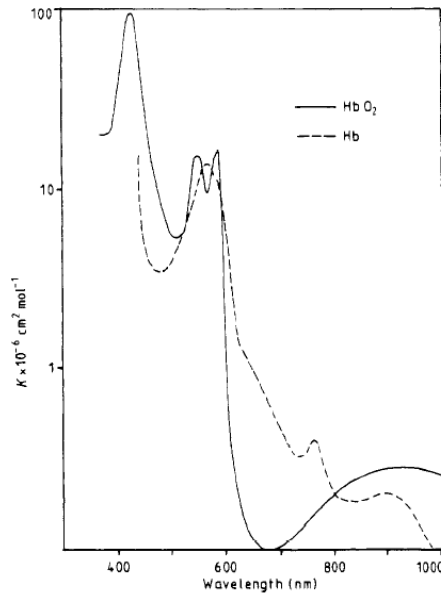


Figure 2: Absorption spectra for HbO₂ and HbO. Maximum difference occurs at about 660 nm. The isobestic point¹ is at 850 nm. (Adapted from ^[1])

The difference between these two curves is important because it is the basis for the non-invasive determination of the oxygen saturation of the blood (SO₂), the ratio of HbO₂ to total haemoglobin in the blood ^[1].

¹ Isobestic point is a specific wavelength at which two (or more) chemical species have the same absorbance^[5]

2.2. The appropriate wavelength

Biological tissues are optically inhomogeneous and are absorbing media with average refractive index greater than one. This refractive index is responsible for partial reflection of the radiation at the tissue/air interface, while the remaining part penetrates the tissue. Absorption and multiple scattering will broaden the incident beam and reduce the intensity of penetration. The scattering events take place mainly in cellular organelles such as mitochondria. Absorbed light is converted into heat or is radiated in the form of fluorescence.

The absorption spectrum depends on the type of predominant absorption centers and water content of tissue. In the ultraviolet (UV) and the infrared (IR) wavelengths light is readily absorbed, which accounts for the small contribution of scattering and inability of radiation to penetrate deep into tissue. Visible light with short wavelengths (green, yellow) penetrates 0.5-2.5 mm and undergoes an exponential decay in intensity. So, it is in this region that scattering and absorption occurs. In the IR and near-IR scattering region photons penetrate approximately 10 mm into the tissue ^[2].

The transmitted light undergoes scattering in the tissue in a very complicated way. Light is refracted in the microscopic inhomogeneities, formed by cell membranes, collagen fibers, and sub-cellular structures. Pigments such as oxyhemoglobin, and bilirubin absorb the diffuse light. It has given the wavelength-dependent absorption characteristics of these pigments. In human skin, the spectral range 600-1600 nm has very good penetration for light. This part of the spectrum is often called the diagnostic window or therapeutic window because it makes deeper tissue layers accessible ^[3].

2.3. The Doppler principle for light-scattering

In LDF, blood flow is measured using the Doppler effect. When a photon interacts with a moving red blood vessel, there is a frequency shift, called Doppler

frequency shift. The size of this shift (ω_d) is determined by the scattering angle (α), the velocity (v) the wavelength of the light in the tissue (λ_t) and the angle (θ) between the direction of the velocity and the scattering vector, as we can see in equation (1). The scattering vector (q) is defined as the difference between the incident light vector (k_i) and the scattering light vector (k_s). The basically principle of LDF is illustrated in figure 3 and in equation 1:

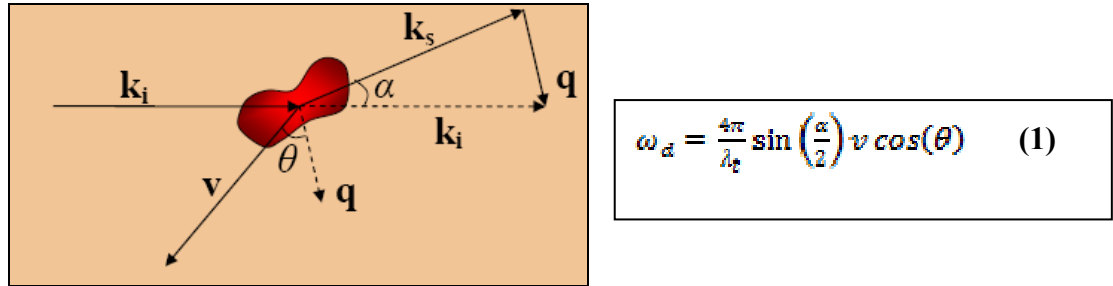


Figure 3: The principle of LDF. (Adapted from^[4])

If we want to quantify the last equation to a typical case ($\lambda=1310$ nm, velocity $v=1$ mm/s, maximum shift), we conclude that the Doppler frequency shift is about 7 kHz. This can be indirectly assessed through the frequency beating phenomenon.

2.4. Frequency beating

Interference phenomenon is a characteristic of coherent light waves.

Since it is obtainable with coherent waves only, a laser source is most suited for this purpose. When the light wave incident in the target is scattered towards the detector the interferometric effect is produced and registered. The Doppler frequency, shifted from the moving red blood cells, the reference frequency of the laser and the beating frequency are all detected in the photodetector. The scattered light from static tissue near the blood vessels is not shifted and is essential to produce the beating frequency in non self-mixing arrangements.

In a simplified one-dimensional situation let us consider two waves propagating along the x-axis with approximate frequencies, $W - \frac{\delta\omega}{2}$ and $W + \frac{\delta\omega}{2}$. These two waves sum with each other.

$$\begin{aligned} \sin\left[\left(k - \frac{\delta k}{2}\right)x - \left(\omega - \frac{\delta\omega}{2}t\right)\right] + \sin\left[\left(k + \frac{\delta k}{2}\right)x - \left(\omega + \frac{\delta\omega}{2}t\right)\right] \\ = 2\sin(kx - \omega t)\cos\left(\frac{\delta k}{2}x - \frac{\delta\omega}{2}t\right) \end{aligned}$$

The result is a wave, modulated in amplitude, propagating along the x-axis. The modulated frequency in this case is $\frac{\delta\omega}{2} = 7\text{kHz}$. This effect can be easily simulated in Matlab as we can see in annex (see Annex A):

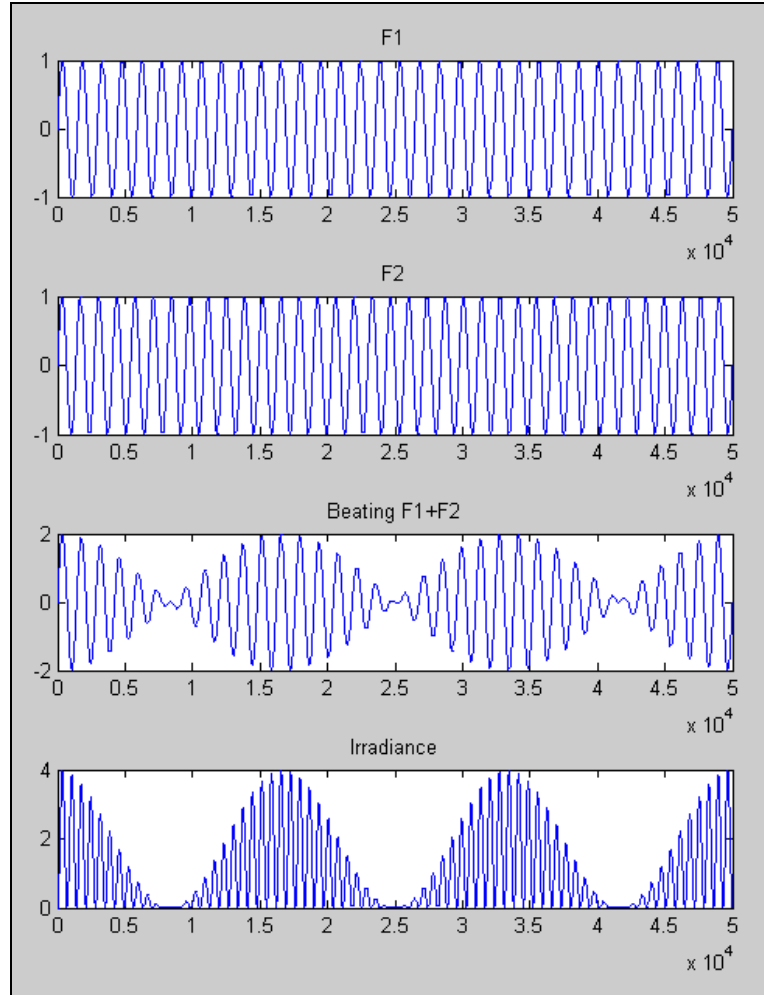


Figure 4: Beating phenomenon of two frequencies F1 and F2. The detector responds to irradiance (last graphic) and because of its time of response it reproduces the covering of this curve.

2.5. Detection

2.5.1. Homodyne

Homodyne detection is a method of detecting frequency-modulated radiation by non-linear mixing with radiation of a reference frequency, the same principle as for heterodyne detection.

In optical interferometry, homodyne means that the reference radiation is derived from the same source as the signal before the modulating process. In laser measurements, the laser beam is split into two parts, one is the local oscillator and the other is sent to the system to be probed. The scattered light is then mixed with the local oscillator on the detector. This arrangement has the advantage of being insensitive to frequency fluctuations of the laser. Usually, the scattered beam will be weaker, in which case the steady component of the detector output is a good measure of the instantaneous local oscillator intensity, and therefore can be used to compensate for any fluctuations in the intensity of the laser. Sometimes the local oscillator is frequency-shifted to allow easier signal processing or to improve the resolution of low-frequency features ^[5].

2.5.2. Heterodyne

Heterodyne detection keeps the principle mentioned above but uses two distinct sources. The reference radiation is known as the local oscillator as mentioned above. The signal and the local oscillator are superimposed at a mixer. The mixer, which is commonly a photodiode, responds to incident energy, thus at least part of the output is proportional to the square of the input ^[5].

Let the electric field of the received signal (E_s) and that of the local oscillator (E_r) be:

$$E_s = E_{s0} \cdot \cos(\omega_s \cdot t + \varphi_s)$$

$$E_r = E_{r0} \cdot \cos(\omega_r \cdot t + \varphi_r)$$

By definition, the irradiance of the detector is proportional to the square of the electric field of the detector:

$$I = \frac{c \cdot \epsilon_0}{2} \cdot [E_{s0} \cdot \cos(\omega_s \cdot t + \varphi_s) + E_{r0} \cdot \cos(\omega_r \cdot t + \varphi_r)]^2$$

$$I = \frac{c \cdot \epsilon_0}{2} \cdot \left[E_{s0}^2 \cdot \cos^2(\omega_s \cdot t + \varphi_s) + E_{r0}^2 \cdot \cos^2(\omega_r \cdot t + \varphi_r) + 2 \cdot E_{s0} \cdot \cos(\omega_s \cdot t + \varphi_s) \cdot E_{r0} \cdot \cos(\omega_r \cdot t + \varphi_r) \right]$$

$$I = \frac{c \cdot \epsilon_0}{2} \cdot \left[\frac{E_{s0}^2}{2} \cdot (1 + \cos(2 \cdot \omega_s \cdot t + 2 \cdot \varphi_s)) + \frac{E_{r0}^2}{2} \cdot (1 + \cos(2 \cdot \omega_r \cdot t + 2 \cdot \varphi_r)) + E_{s0} \cdot E_{r0} \cdot [\cos((\omega_s + \omega_r) \cdot t + (\varphi_s + \varphi_r)) + \cos((\omega_s - \omega_r) \cdot t + (\varphi_s - \varphi_r))] \right]$$

By filtering out, the low-frequency components are eliminated:

$$I = A \cdot \left[\frac{1}{2} \cdot (E_{s0}^2 + E_{r0}^2) + E_{s0} \cdot E_{r0} \cdot [\cos((\omega_s - \omega_r) \cdot t + (\varphi_s - \varphi_r))] \right]$$

The photocurrent has a DC component proportional to the total irradiance and has a frequency beating component $(\omega_s - \omega_r) = 2\pi\Delta f$. With suitable signal analysis the phase of the signal can be recovered, too.

Hence, if we plot the spectrum of intensity in the detected signal against frequency we obtain a picture similar to figure 5.

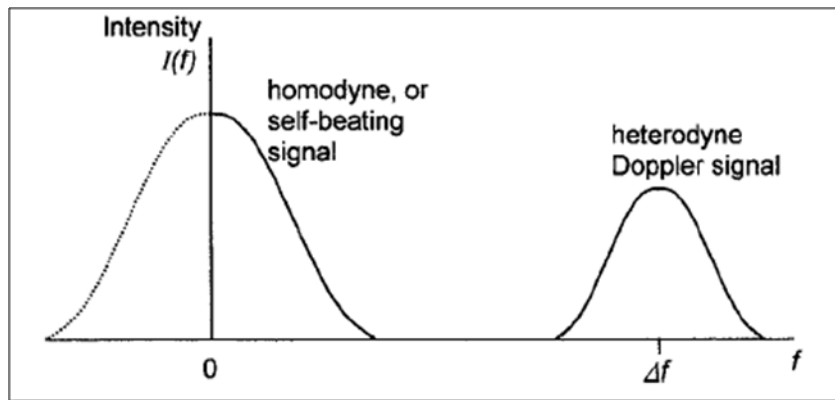


Figure 5: Homodyne and Heterodyne Doppler signals. (Adapted from ^[6])

2.6. Light Transportation

2.6.1. Free space

Transportation of both, transmitted and received light, in free space means that no optical fibers are used, neither for illumination or signal detection. An example is depicted in figure 6.

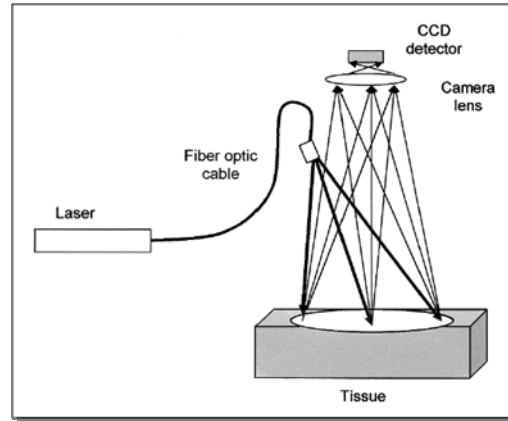


Figure 6: Schematic diagram of laser Doppler in free space using fiber optic cable. (Adapted from ^[7])

2.6.2. Fibers

In 1977, Holloway & Hatkin's were the first to use optical fibers to return laser power and to collect Doppler shifted of backscattered light.

There are two kinds of optical fibers that can be used for light transportation, multimode and single-mode:

a) Multimode fibers

Multimode fibers were the first to be commercialized and are mostly used for communication over short distances. Because multimode fibers have a larger numerical aperture than single-mode fibers, they support more than one propagation mode, hence they are limited by modal dispersion, where single-mode fibers are not. Consequently multimode fibers have higher pulse spreading rates than single-mode, limiting transmission capacity ^[5]. Also, they have higher “light-gathering” capacity (the larger core size simplifies connections and also allows the use of lower-cost electronics).

b) Single-mode fibers

Single-mode fibers are designed to carry a single mode of light. Unlike multimode fibers, single-mode fibers do not exhibit dispersion resulting from multiple spational modes. Single-mode fibers are also better at retaining the fidelity of each light pulse over long distances than are multimode fibers. For these reasons, single-mode fibers can have a higher bandwidth than multimode fibers. Equipment for single-mode fiber is more expensive than equipment for multimode fiber.

To illustrate these considerations, in figure 7 an example of an instrument that uses laser Doppler technique to measure blood perfusion is shown. It uses single-mode fibers to illuminate and multimode fibers to capture.

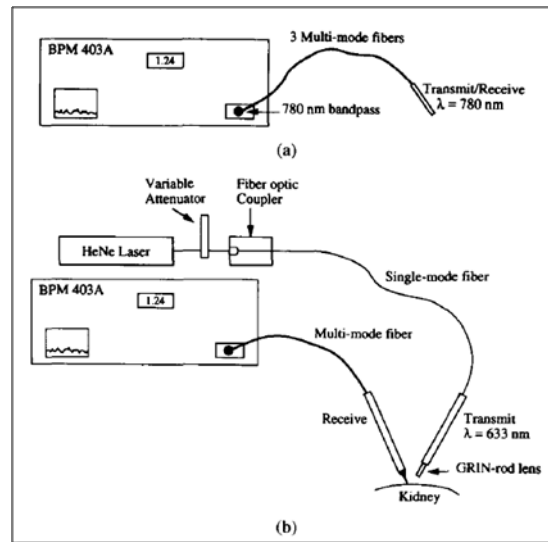


Figure 7: a) Blood perfusion monitoring using three multimode fibers as transmit and receive of light. b) Current laser Doppler velocimeter using single-mode fiber for transmit light and multimode fiber for receive light. (Adapted from ^[8])

To prove the last considerations W. M. Wang ^[9] made experiments with both single-mode and multimode fibers. They are applied to self-mixing interference in a diode laser. The results showed comparatively few differences between the fibers: the multimode fiber was easier to align, had a higher signal-to-noise ratio, implied lower costs and made it easier to obtain a higher coupling efficiency. However, it was more

sensitive to the environmental change to be measured. The single-mode fiber showed the opposite properties.

2.7. Output

2.7.1. Laser Doppler Flowmetry

Laser Doppler Flowmetry (LDF) is a continuous and non-invasive method for tissue blood flow monitoring, utilizing the Doppler shift of laser light as the information carrier. This subject will be discussed in more detail in chapter 3. Figure 8 shows a typical LDF output.

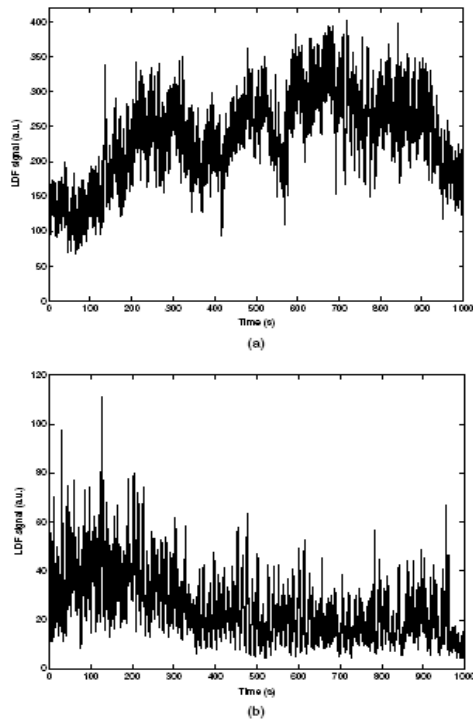


Figure 8: a) Signal of LDF output in a healthy patient. b) Signal of LDF output in a diabetic patient.

(Adapted from ^[10])

2.7.2. Laser Doppler Imaging

Laser Doppler Imaging (LDI) is a non-contact method for visualization of spatial and time blood flow dynamics.

In figure 9 a LDI implantation is represented.

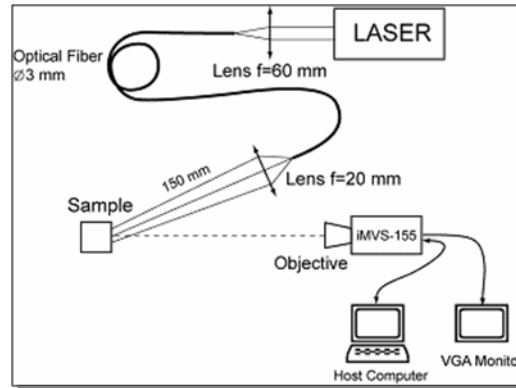


Figure 9: Schematic of LDI. (Adapted from ^[11])

The two-dimensional false-color maps of the blood flow are displayed on the computer monitor, as shown in figure 10.

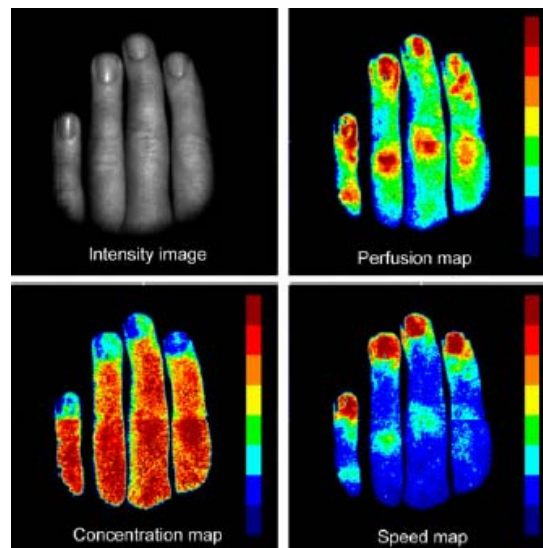


Figure 10: Blood flow-related images of human fingers. (Adapted from ^[12])

In contrast with conventional LDF which measures a single point, functional mapping images not only correlate in magnitude with the degree of perfusion, but also locate changes of blood flow with high spatial specificity.

2.8. Self-mixing

The simpler way to obtain the interferometric effect that gives rise to the Doppler effect is by means of the so-called self-mixing geometry.

The self-mixing effect in a laser diode was first observed and used for Doppler measurements from solid moving objects by Sinohara *et al* ^[13] almost 20 years ago. In the early 1990s the technique was applied to blood flow velocity measurements via fiber-coupled laser diode by Slot *et al* ^[14] and for direct liquid flow measurements and blood perfusion by the Mul *et al* ^[15].

A self-mixing effect in a laser occurs when some part of the emitted laser light enters back into the laser cavity, where it interacts with the original laser light, causing fluctuations to the laser power. These power fluctuations can be detected using a diode placed on the opposite side of the laser cavity. If the external light is frequency-shifted and it is mixed coherent to the original laser light, interference occurs and this can be superimposed to many measurement applications such as blood perfusion ^[16].

2.8.1. Theory of self-mixing interferometry

The most common way of explaining the signal generation in self-mixing interferometry is a three-mirror Fabry-Perot. The schematic arrangement of the self-mixing effect is presented in figure 11. Two mirrors R_1 and R_2 constitute the laser cavity. The moving object can be presented as a third mirror R_3 . The light reflected from the target interfered with the light at the laser front facet with different phase swift determined by the distance to the target. Mirror R_3 and one of the laser facets, R_2 constitutes an effective laser mirror R_e , the reflectivity of which depends on the distance. The dependence of effective reflection from the second laser mirror on the length of

external cavity causes changes in the threshold of generation and the output light power of the laser. It is clear that the laser optical output includes a modulation term dependent on the feedback strength and the distance of the external reflector. It corresponds to a variation of the $\lambda/2$ displacement at the external reflector and it is a repetitive function with a period of 2π rad. This model is based on coherence of light inside the external cavity.

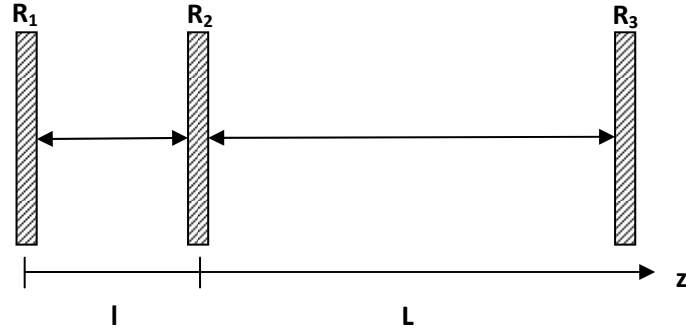


Figure 11: Three-mirror cavity model used to analyze the optical feedback configuration; R_1 and R_2 are the laser mirror reflectivities, R_3 is the external (target) reflectivity, l is the laser-cavity length and L is the distance from laser-cavity front face to target.

According to the three-mirror model ^{[17][18][19]} the field in the laser cavity can be calculated by applying the amplitude and phase criteria for the stationary state of the light, propagating in the laser cavity. The changes, in threshold gain and therefore in the optical output variations ΔP due to feedback, were shown to have a dependence on the length of the external cavity:

$$\Delta P \propto \frac{1 + R^2}{Rl} R_{\text{ext}} \cos \omega_d \tau_{\text{ext}}$$

Where R is reflectivity of the laser facets, l is length of the laser cavity, R_{ext} is reflectivity of the moving object, ω_d is the lasing frequency with optical feedback, $\tau_{\text{ext}} = \frac{2L}{c}$ is the round-trip time of the laser light in the external cavity, c is the speed of light and L is the distance from the front facet of the laser cavity to the moving object.

When the target moves, the reflected or scattered light contains a frequency shift, which is proportional to the velocity of the moving target. According to the Doppler theorem, the Doppler frequency is:

$$\omega_d = \frac{4\pi}{\lambda_t} \sin\left(\frac{\alpha}{2}\right) v \cos(\theta)$$

Substituting this to the previous equation it can be seen that the power fluctuations of the laser diode are related to the Doppler frequency. Thus, it is possible to determine the velocity of the target measuring these power fluctuations.

3. State of the art

In this chapter, an outline of the development of the LDF and the current status of some available instruments for assessing blood perfusion will be made.

3.1. Laser Doppler Flowmetry (LDF)

As described before, LDF is a non-invasive method to measure the blood perfusion of human tissue. The principle of LDF is drawn in figure 12. A laser transmits photons into the tissue, which are scattered and reflected. Every photon that meets a moving blood particle undergoes a shift in frequency. A photodiode receives the photons leaving the tissue and converts them into current. The Doppler shifted photons causes an AC current on top of the DC current from the non shifted photons. The frequency spectrum of the AC current gives information about the Doppler shift and thus the blood perfusion of the tissue.

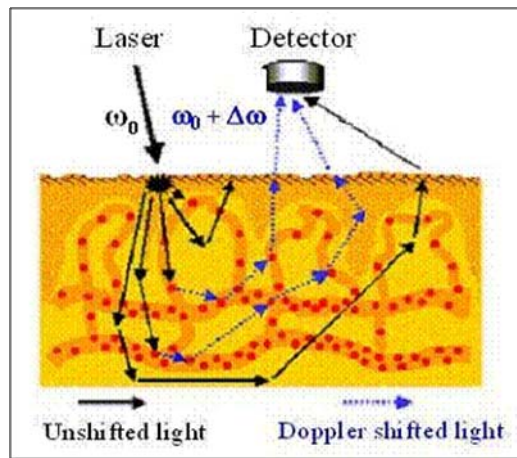


Figure 12: Basic principle of LDF. (Adapted from ^[20])

The perfusion in the skin relates the blood flow in the microcirculation. Microcirculation is composed of capillaries, arterioles, venules and shunting vessels. The perfusion through capillaries refers to the nutritive flow, whereas flow through the other mentioned vessels refers to the temperature regulation flow, and also feed and drain the

capillary network. However, skin perfusion can be impaired by diseases. These impairments can lead to ulcer formations as well as necrosis. Monitoring skin blood perfusion in real time, continuously and non invasively is possible with the LDF technique, that is of great importance in clinical routine.

3.1.1. Units

Currently, LDF does not give an absolute measure of blood perfusion. Strictly speaking, perfusion implies the amount of fluid being moved per unit time (ml/sec. /vol.) rather than the mere velocity. Measurements are expressed as Perfusion Units (PU) which are arbitrary units. For the clinical apparatus this is a limiting factor and the reason why LDF instruments are not routinely used in health care.

To enable comparison of results, it is necessary to calibrate the laser Doppler flowmeters. PeriFlux was the first to develop a special utility standard for this propose [22].

3.1.2. Applications

LDF has found its use essentially in research. Among the applications are pharmacological trials, allergy patch testing, wound healing, physiological assessments and skin disease research [23]. Some areas of major interest for LDF studies are the following [22].

- Cochlear blood flow
- Neurological applications such as peripheral nerves and CNS blood flow
- Kidney and liver blood flow
- Skeletal muscle studies
- Bone blood flow studies
- Skin blood flow studies: effect of local anesthesia, skin physiology, provocation studies, skin pharmacology studies
- Plastic surgery

- Obstructive and occlusive diseases
- Odontological studies
- Retinal blood flow
- Gastrointestinal blood flow

3.2. Literature

Laser Doppler has been used to measure blood flow since the 70's. It was first applied on retinal blood flow (Riva *et al.* 1972) but was soon extended to other tissues (Stern *et al.* 1975). Stern was the first to demonstrate that signals related to blood flow could be obtained non-invasively using the Doppler effect. He used a helium-neon laser as a light source and a photomultiplier tube as a light detector. Then, solutions for the difficulties related with light scattering had to be found.

Since then various models have been proposed, starting with the pioneer work of Watkins & Holloway (1978). A number of clinical and experimental applications of LDF have been implemented (Nilsson *et al.* 1980, Bonner & Nossal 1981), Shepherd & Riedel 1982, Nilsson 1990). In addition, the laser Doppler technique has been applied to laser Doppler microscopy (Mistrina *et al.* 1975, Priezzhev *et al.* 1997) and perfusion imaging (Wardell *et al.* 1993)^[16] which detects blood flow from a large tissue area. This is useful when spatial information about flow is required, rather than its dynamical properties.

Later, other applications have been developed such as dental diagnosis (Roebuck *et al.* 2000), vitality assessment in skin and bone exerts (Wong 2000), perfusion measurement during liver transplantation (Ronholm *et al.* 2001), diabetic assessment alterations in microcirculation (Meyer *et al.* 2001) and diagnosis of deep vein thrombosis (de Graaf *et al.* 2001)^[6].

Recently laser Doppler has been objective of study, combination with the new technique of optical coherence tomography (OCT). When combined with Doppler, it is possible to measure blood flow at specific depths inside tissue.

LDF technique, its applications and its examples can be found in the literature, mostly in two important books (Belcaro *et al.* 1994) and (Shepherd *et al.* 1990).

LDF offers a lot of advantages when compared with other methods relatively to blood flow measurement in microcirculation. Various studies show that this is a method with high sensitivity and high responsivity to local blood perfusion and it is a versatile and easy method for continuous measurements. Moreover, it is a non-invasive method so it will never jeopardize the normal way of working of the microcirculation of the patient [21].

The methodology is, nowadays, used in various medical and chirurgical applications such as visualization of skin tumors, diabetes, obstructive and occlusive diseases, ischemia and others.

3.3. Commercial instruments

There are many types of equipment to measure blood perfusion. Three of the most known commercial instruments are the DTI Oxylab LDF, the Oxyflo and PeriFlux. The images of these equipments are shown in figure 13.



	<p>OXYFLO 'OxyFlo2000' / 'OxyFlo4000' 2 or 4 channel laser Doppler tissue blood perfusion monitor</p>
	<p>OXYLAB^{LDF} 'OxyLab LDF' Single channel laser Doppler tissue blood perfusion monitor</p>



Figure 13: Commercial instruments used to measure LDF. (Adapted from ^[21]^[22])

The specifications of both DTI Oxylab LDF and the Oxyflo instruments are shown in annex B.

The DTI Oxylab gives LDF signal and information about the oxygen pressure and the temperature from the same tissue site too. Figure 14 shows an example of DTI Oxylab output.

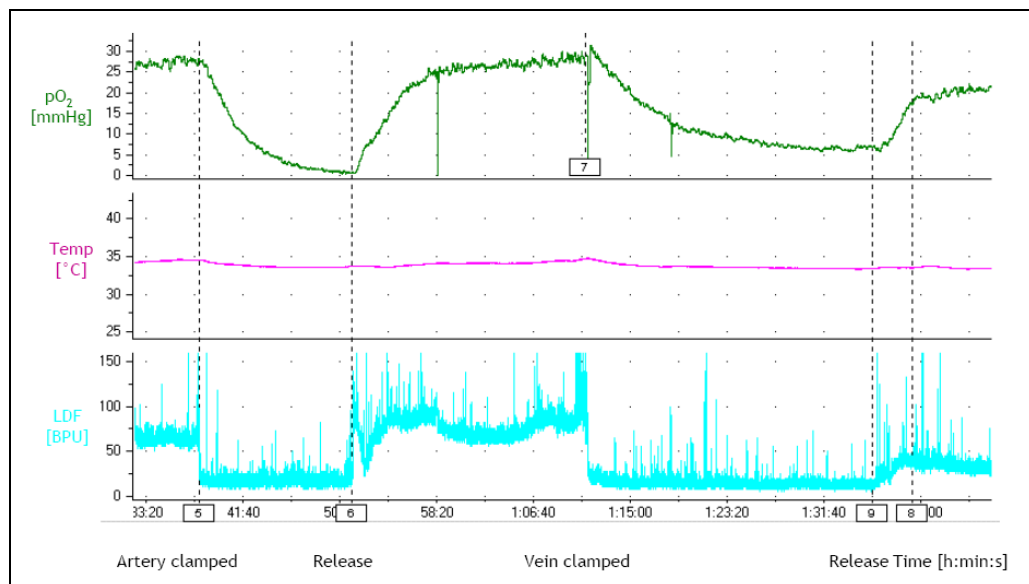


Figure 14: Example of DTI Oxylab output. (Adapted from ^[21])

From the PeriFlux, several different types of signal can be obtained, such as perfusion, concentration of moving blood cells (CMBC), temperature and velocity. Perfusion represents the product of the velocity and the CMBC within the measuring volume.

The PeriFlux allows evaluation of microvascular perfusion in real-time. The technique can be either non-invasive or invasive, depending on the tissue under study. With a multi-channel PeriFlux system, perfusion measurements can be made in up to six different sites simultaneously ^[22].

4. Self-Mixing

We used the self-mixing because its main advantage, where compared to conventional interferometers is that the measurement set up is simple since it deals with only two optical components, the laser diode and the optical fiber. This technique is best suited when light is coupled to an optical fiber as is the case in pig-tailed laser diodes. It also lends itself to a very simple, yet effective, way of building an experimental set up. Moreover, the Industry manufactures these two components as a single pack – the pigtailed laser diode – that comes pre-aligned in a variety of wavelengths (635 nm to 1550 nm) and output powers (1 to 100 mW) .

An important study was drawn by Wang ^[9] that reaches the conclusion: the self-mixing effect does not depend on whether the fiber used to couple is a single mode or a multimode, which is plus an advantage of the method.

One obvious disadvantage of self-mixing results from its inherently punctual nature which is quite inappropriate for imaging purposes.

In this work a laser was used to send light through a pigtailed laser diode to a movable target from which light backscattered was detected. The order of magnitude of the frequency beating values in self-mixing geometry will be estimated in section 6.1. and the results will be presented in section 6.2.

Prior to this stage it was also introduced an avalanche photodiode (APD), just as an alternative method to self-mixing, but we didn't proceed making measurements with it because the self-mixing method seemed to be more appropriated. However, ADP has a higher gain that might be useful in some applications.

5. Experimental Setup/Bench Tests

In this chapter, the operation basic principle of the system will be introduced. A description of the measurement probe, the interface system, the data acquisition and signal processing will be made. The experiments on the self-mixing arrangement for LDF with a loudspeaker and a moving strip will also be described.

5.1. Schedule

The following schedule synthesizes my work done since August 2006 till September 2007:

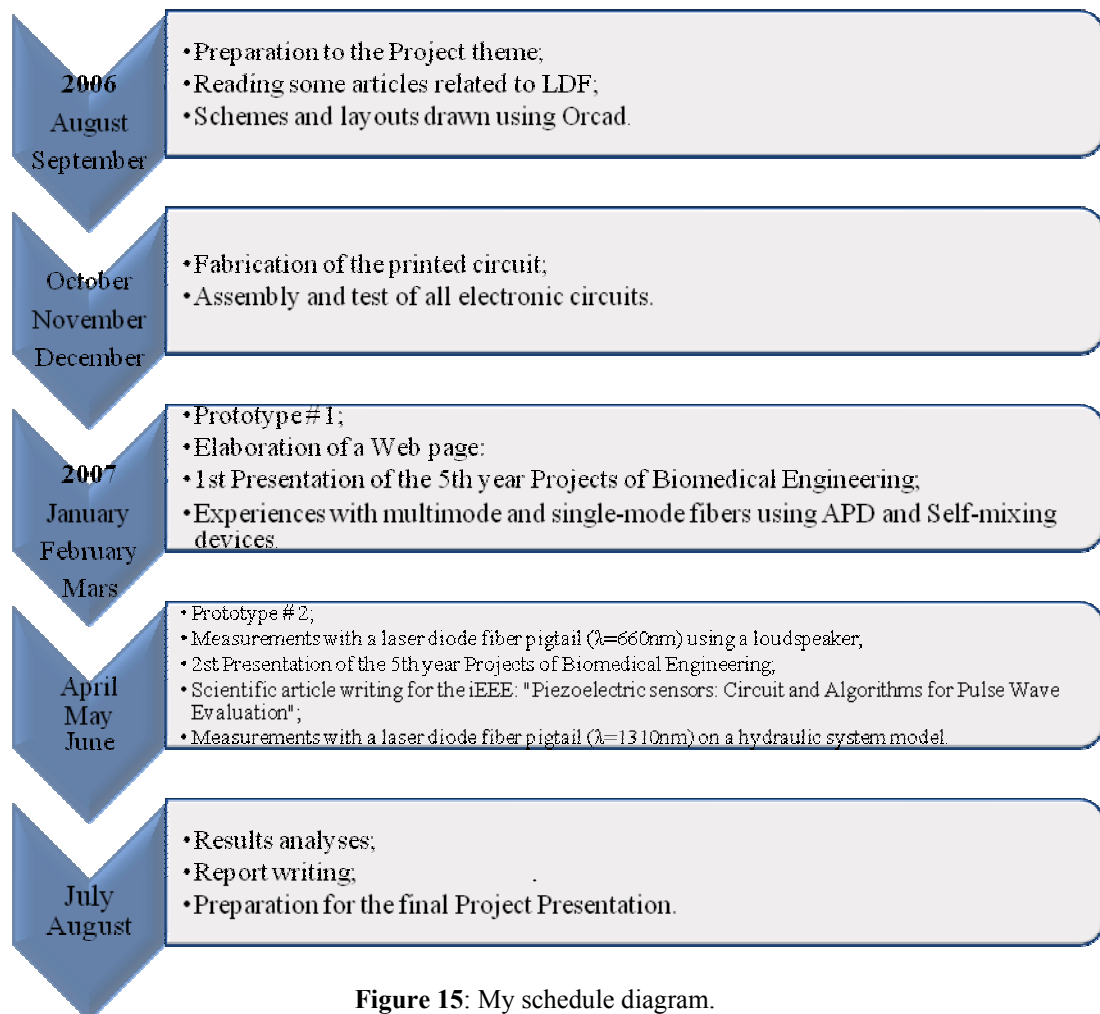


Figure 15: My schedule diagram.

5.2. System Architecture

The developed laser Doppler measurement system can be divided into different blocks, shown in figure 16. These are: 1) the laser Doppler probe where a self-mixing interferometer is implemented; 2) the interface system, which contains the laser driver, the power supply; 3) the USB6009 board, from National Instruments, for data control; 4) and, at last, the data acquisition and signal processing, computing system.

The circuit board provides all necessary resources for the realized applications so far.

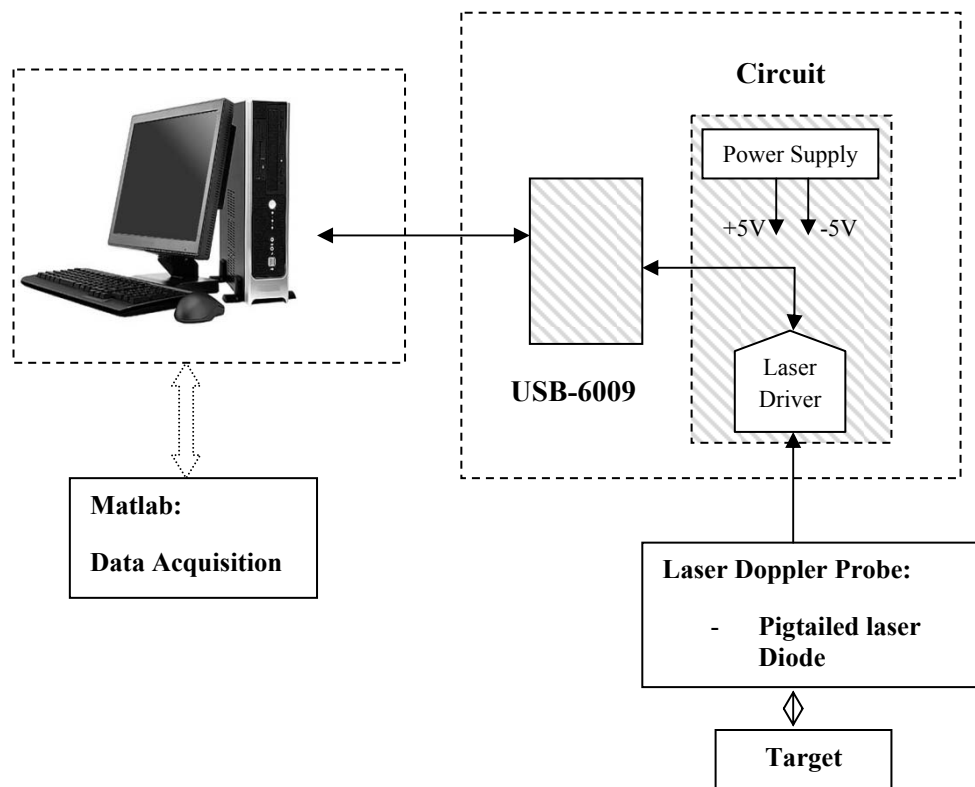


Figure 16: Block diagram of the complete system.

5.2.1. Measurement probe

The experiences, using prototype 2, were due to the non successful sequence of experiences made before, using prototype 1. These are illustrated in figure 17.

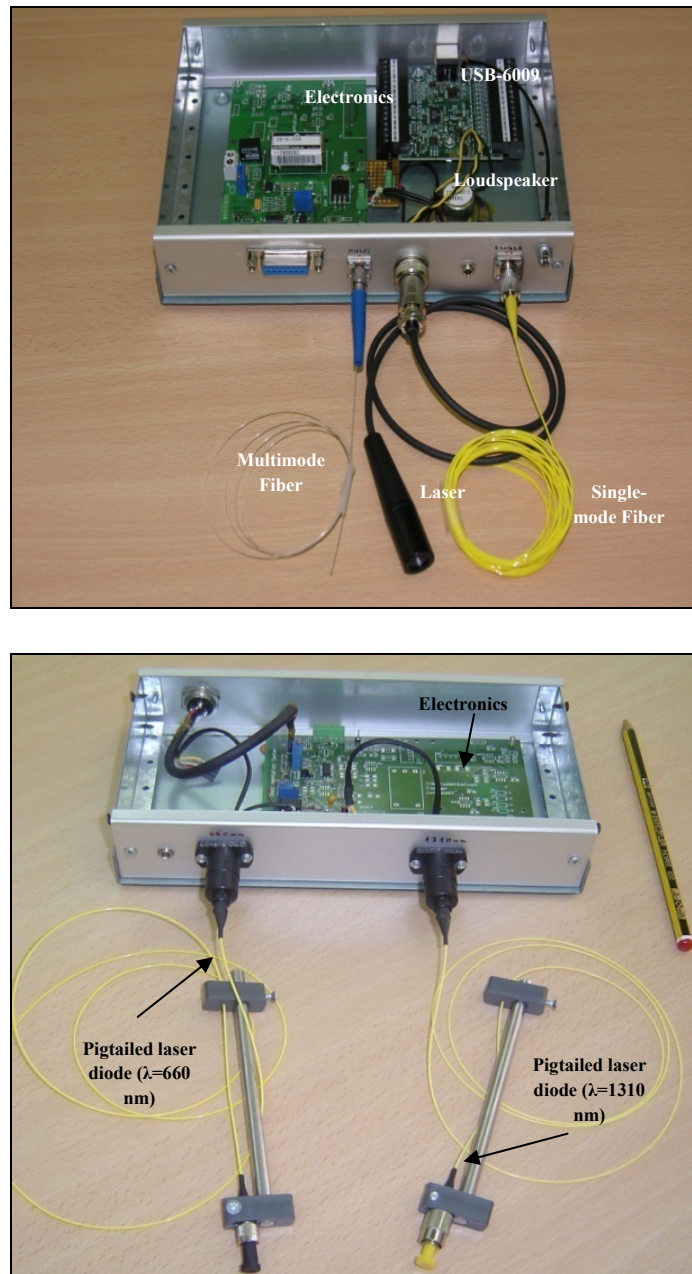


Figure 17: Prototypes 1 (top) and 2 (bottom).

At the beginning, the LT230220P-B (an optical Laser Package with a focusing tube with C230220P-B optic) pair was used to impinge light to the target. Here, we have been confronted with diffraction problems caused by the system optical aperture. So, the focusing tube was replaced by a collimation tube, the LT220P-B. Both assemblies are schematized in annex C.

Further, experiments were made using multimode and single-mode fibers as light conveyors. Like Wang ^[9], we concluded that the self-mixing effect does not appear to depend on whether the fiber used to couple the source to the target is single-mode or multimode.

The use of prototype 1 was then abandoned and a new prototype, prototype 2, incorporating a pigtailed laser diode was put in use. The pigtail solution provides good coupling efficiency between the laser diode and the fiber, and as an additional advantage of this design, should the diode ever fail, it could be easily replaced while reusing the rest of the optics.

Two important experimental studies of self-mixing interferometry were performed before trying the biomedical measurements. Bench Test I is about the test of the self-mixing effect using a loudspeaker, and Bench Test II is about the same using a moving strip.

5.2.2. Interface system

5.2.2.1. Circuit

The printed circuits were elaborated with the help of OrCAD®. This tool offers PCB designers, the power and flexibility to create and share PCB building data. OrCAD® layout delivers all the capabilities designers need, from netlist, to route and place. The PCB design of the LDF work is illustrated in annex D.

The printed circuit has double face, has plated through holes and has a mask solder.

The electrical and electronic circuit components were then mounted and the results were already shown in figure 17.

The circuit has two essential constituents, the Power Supply and the Laser Driver. The Power Supply is $\pm 5V$ because these values are compatible with the specifications of the components, particularly those of the OpAmps. The Laser Driver is constituted by 5 main blocs, as it can be seen in annex E. They are:

- Dual Polarity Current Source

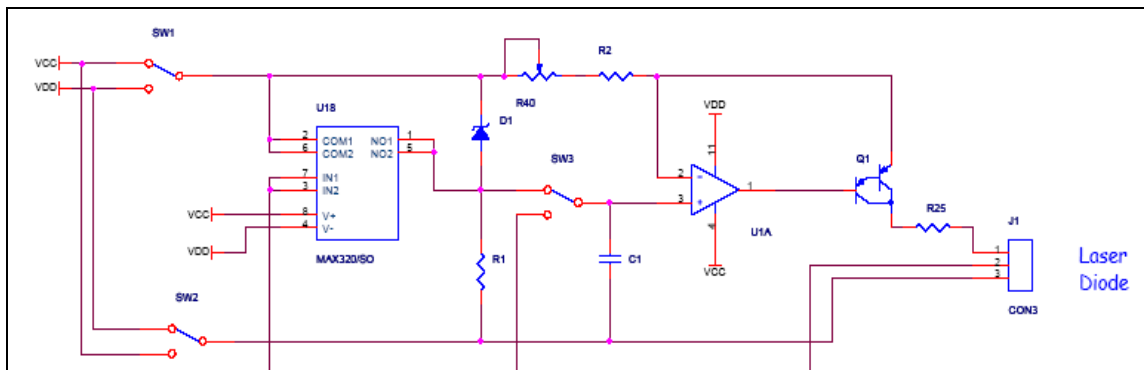


Figure 18: Schematic of the dual polarity current source.

The scheme depicted in figure 18 is due, essentially, to provide dual polarity current to activate the laser diode. The components that must be noted are:

- The darlington Transistor (Q1). It gives a high current gain to the circuit. Because it works as a dual polarity current source, it can be a PNP if it works as a current source (see figure 18) or a NPN if it works as a current sink. In this last case the switches SW1 and SW2 must be set, differently.
- The trimmer (R40), a variable resistor component allowing making fine adjustments to its resistance, to control the current;
- MAX320/SO (U18), an electric switch which allows lighting the laser in a progressive way. If it is in closed, the Zener diode (D1) has no current and the laser turns off, otherwise the Zener conducts and the laser turns on.

- The Transconductance Amplifier

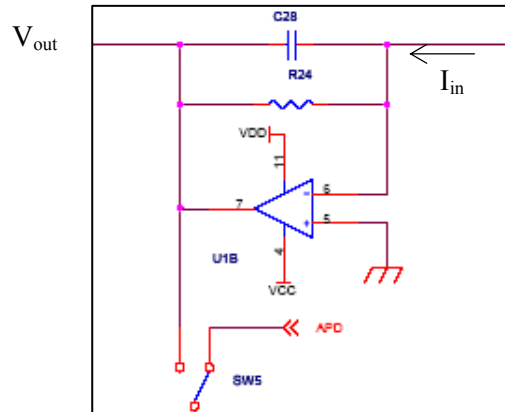


Figure 19: Schematic of the transconductance amplifier used in laser driver circuit.

- The Transconductance Amplifier/ Voltage Follower

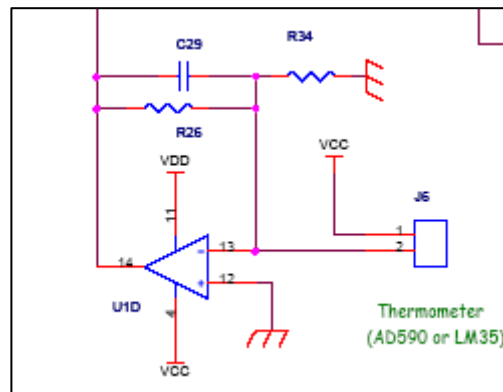


Figure 20: Schematic of the voltage follower. If we take off R₃₄ it becomes a transconductance amplifier.

The block of the figure 20 corresponds to a voltage follower, however, without R₃₄ it becomes to a transconductance amplifier.

- The Audible Monitoring

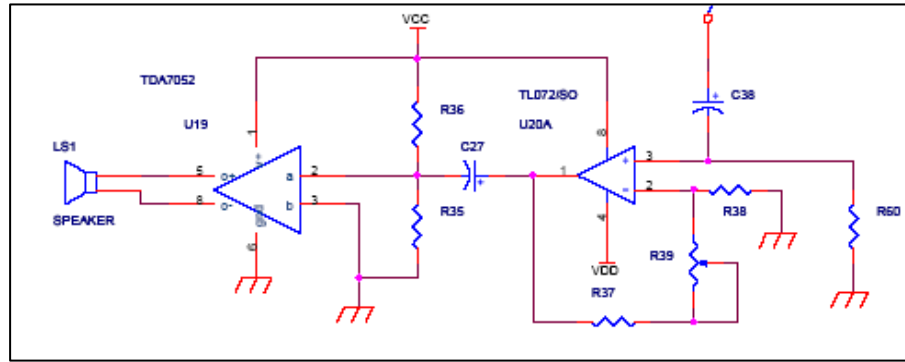


Figure 21: Schematic of the audible monitoring.

- The DC-DC Converter

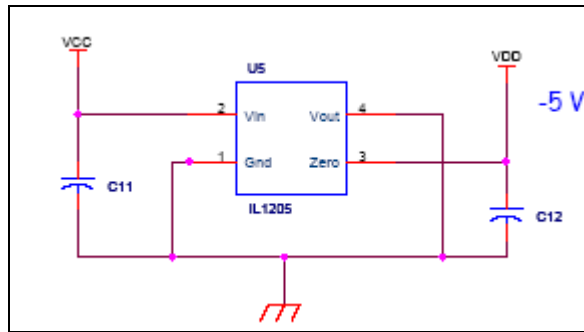


Figure 22: Schematic of the DC-DC Converter.

5.2.2.2. USB-6009



Figure 23: NI USB-6009. (Adapted from [23])

The National Instrument USB-6009 multifunction data acquisition (DAQ) module showed in figure 23 provides reliable data acquisition at low price. With plug-and-play USB connectivity, this module is simple enough for quick measurements but versatile enough for more complex measurement applications. The NI USB-6009 uses NI-DAQmx high-performance and multithreaded driver software for interactive configuration. All NI data acquisition devices shipped with NI-DAQmx also includes the VI Logger Lite, a configuration-based data logging software package. The USB-6009 has removable screw terminals for easy signal connectivity. It is ideal for a number of applications such as:

- Data logging – Log environmental or voltage data quickly and easily;
- Academic lab use.

The specifications of the Low-Cost Multifunction DAQ for USB are described in annex F. Some of them are:

- 8 analogue inputs (14-bit, 48 kS/s);
- 2 analogue outputs (12-bit, 150 S/s); 12 digital I/O; 32 bit counter;
- Bus-powered for high mobility; built-in signal connectivity;
- Compatible with LabVIEW, LabWindows/CVI, and Measurement Studio for Visual Studio.NET.

5.2.3. Data acquisition and signal processing

The data acquisition and signal processing are done with a PC. As mentioned before, the board interfaces easily with Matlab. We choose Matlab to be equipped with the Data Acquisition Toolbox 2.9 that provides a set of tools for analogue input, analogue output and digital I/O from a variety of PC-compatible data acquisition hardware. The toolbox supports a lot of popular hardware devices, but we are interested in National Instruments boards that use Traditional NI-DAQ or NI-DAQmx driver software ^[24].

Specifically for the present application, a Matlab program was created to study LDF data acquisition. This program is in annex G. The flowchart in figure 24 demonstrates how the Matlab programmer provides visualization of the LDF signal.

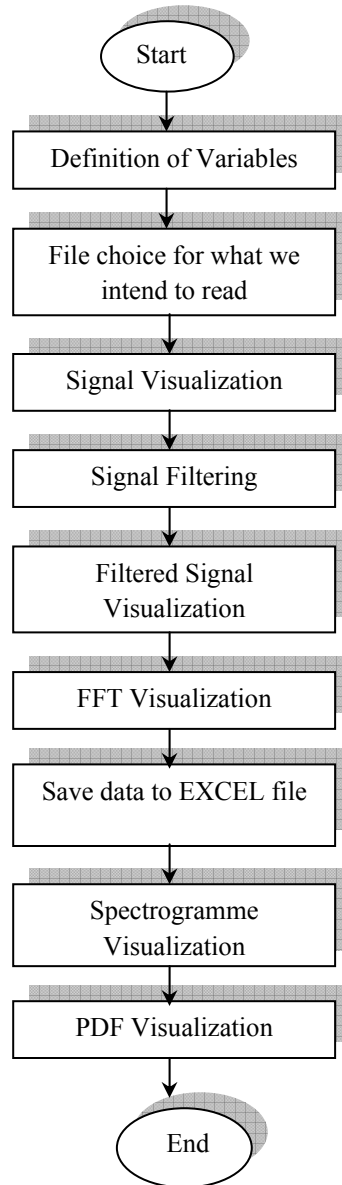


Figure 24: Flowchart of the Matlab programmer.

The Doppler signal analysis is based on Fast Fourier Transform (FFT) calculation. This is done because in the time domain it is very difficult to calculate fringes due to fluctuations.

It is possible to relate the Probability Density Function (PDF) with the Doppler frequency spectrum. This subject will be discussed, in more detail, in section 6.

5.3. Bench Test I

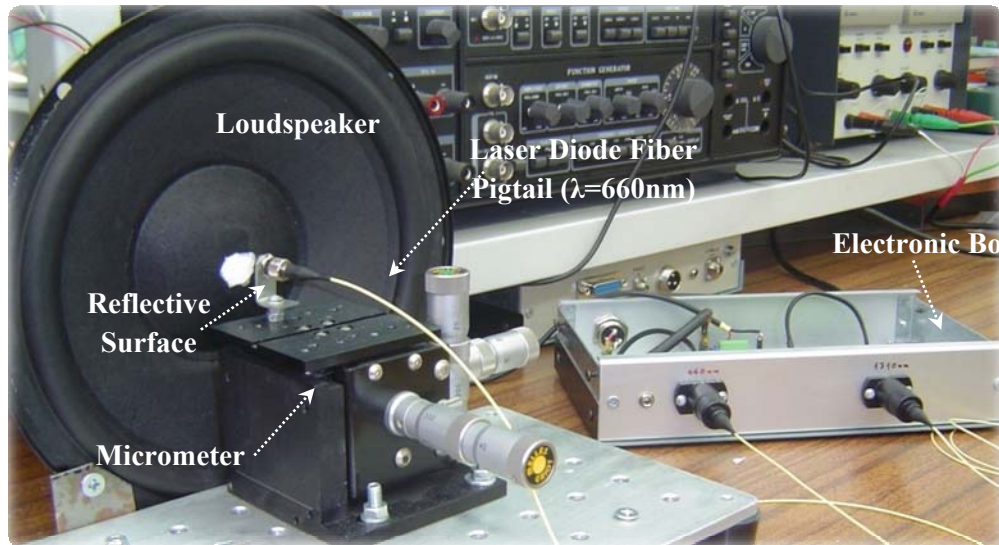


Figure 25: Image of the experimental arrangement I for LDF detection.

The experimental arrangement related to the loudspeaker setup is showed in figure 25.

A Pigtailed laser diode (LPM-660-SMA) with a wavelength of 660 nm, with an output optical power 22,5mW and a multimode optic fiber were used in the experiment. The light from the pigtail was emitted from the fiber and reflected back into the laser cavity via the same fiber. A reflective surface attached to a loudspeaker cone driven by a

signal generator was used as a target, to provide phase variations of the external optical feedback.

The HL6501MG diode laser package incorporates a photodiode (PD) accommodated in the rear facet to monitor the laser power. This characteristic of the device is particularly well suited to observing the self-mixing interference, and it provides a convenient internal detector. The end of the fiber was fixed at 45 degrees angle, near to the reflective surface. The distance from the fiber end to the reflective surface was about 2 mm. A PC with Matlab data acquisition (see section 5.2.3) was used to record the output signal.

A total of 40000 samples were recorded for each period over a time of nearly 5 seconds. The voltage amplitude feeding the loudspeaker's membrane was constant, with the value of 10 mV. The purpose was to vary the modulated frequency and observes the changes in the Doppler spectra.

5.4. Bench Test II

The experimental arrangement related to the moving strip setup is showed in figure 26.

In this bench test, the light from the Pigtailed laser diode (LPS-1310-FC, single-mode fiber) with a wavelength of 1310 nm and with an output optical power of 2,5 mW, was emitted from the fiber and reflected back into the laser cavity via the same fiber. As a reflective surface it was used a white paper strip, because it was highly scattering such as the human skin. The target was moved at a certain velocity. The end of the fiber was fixed at a 45 degrees angle, near to the moving strip, and the distance from the fiber end to the moving strip was about 1 mm, as showed in figure 26. Then, the output signal was recorded with a PC with the Matlab data acquisition tool, mentioned before.

A total of 40000 samples were recorded for each period over a time of nearly 5 seconds. The strip movement is repeated for increasing velocity regimes. The purpose was to vary the velocity and observe the changes in the Doppler spectra.

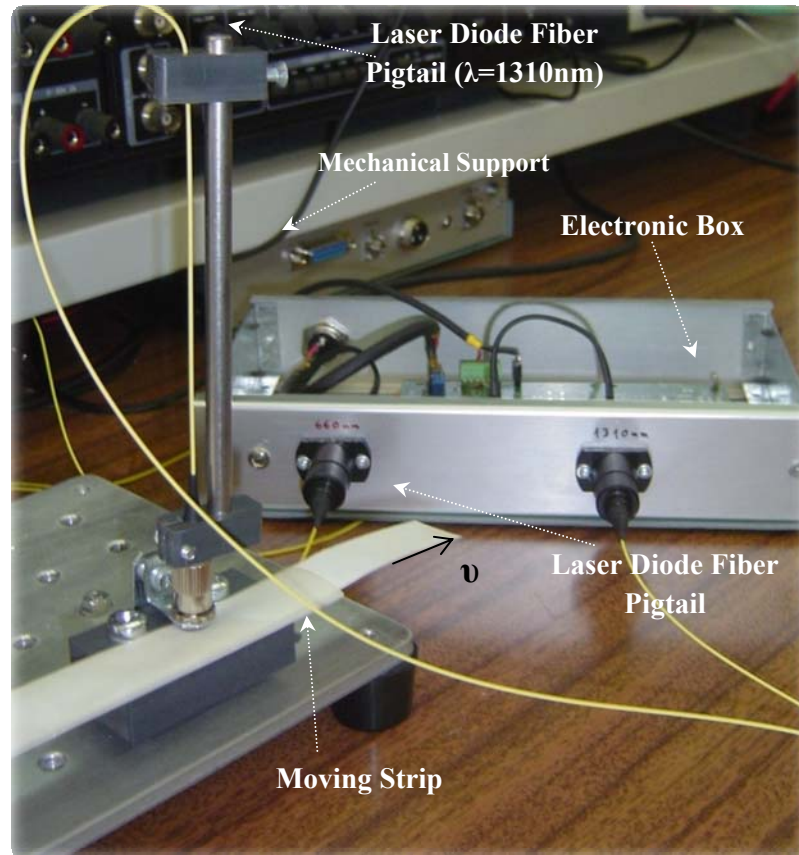


Figure 26: Image of the experimental arrangement II for LDF detection.

6. Results

In this chapter, a dimensioning of theoretical background will be made. The results of the experiments on the self-mixing arrangement for LDF with a loudspeaker will be presented. Suggestions for future work will also be drawn.

6.1. Dimensioning

In this section the order of magnitude of the frequency beating values will be estimated for the self-mixing geometry that we are studying and has been reviewed in sections 2.8. and 4.

As was referred in section 2.3, the Doppler effect is based in a frequency shift, ω_d , expressed by the equation (1). Recalling that angles α and θ were defined as

$$\alpha = [\vec{K}_i, \vec{K}_s] \quad \theta = [\vec{v}, \vec{q}]$$

we will now estimate ω_d for this geometry based on figure 27 where $\alpha \approx \pi$ and $\theta \approx 0$.

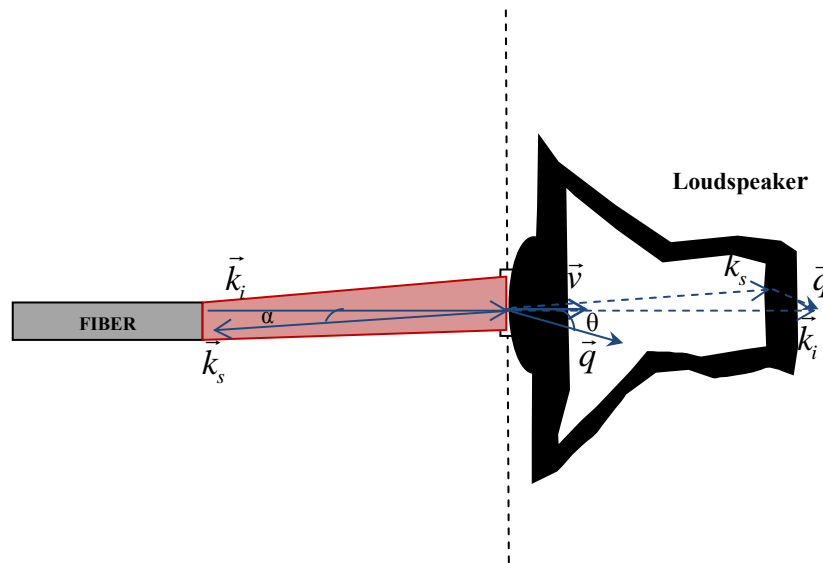


Figure 27: The loudspeaker arrangement.

Substitution of this values in equation (1), leads to:

$$\omega_d = \frac{4\pi}{\lambda_t} \sin\left(\frac{\pi}{2}\right) v \cos(\theta) = \frac{4\pi}{\lambda_t} \Rightarrow \omega_d \text{ max}$$

In our case the wavelength (λ_t) and the velocity (v) are respectively 660nm and about 1mm/s. So we can expect that the maximum Doppler frequency shift is around 19 kHz.

In fact, we can conclude that the fiber tip and the loudspeaker should be perpendicular to each other if we want to obtain the maximum Doppler shift.

Figure 28 depicts the moving strip setup.

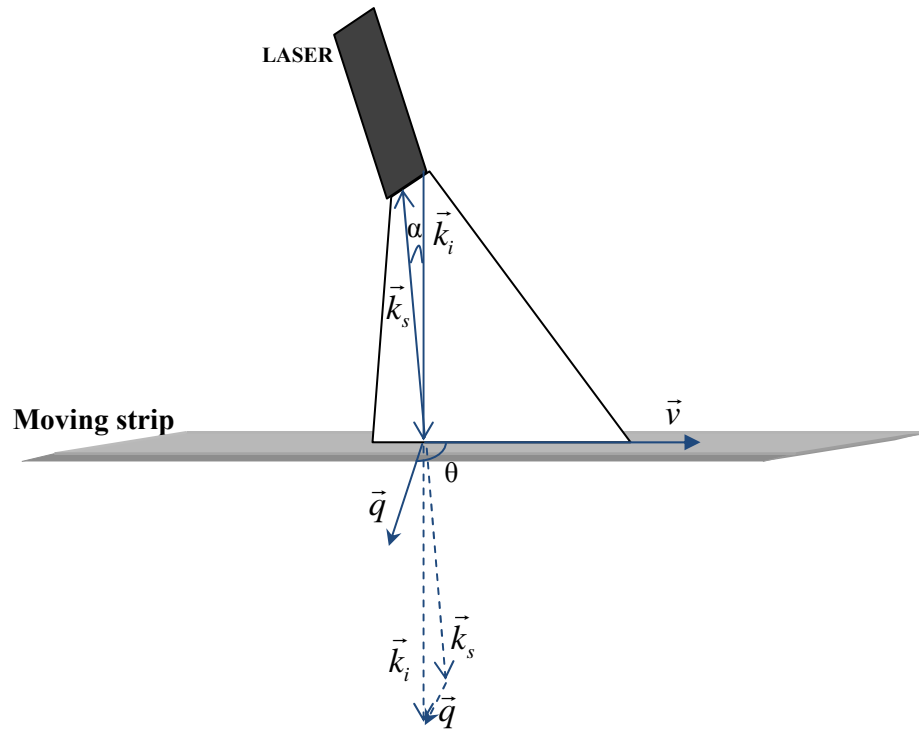


Figure 28: The moving strip arrangement.

In this case, $\alpha = \pi$ and $\theta = \frac{\pi}{2}$. Taking these values into equation (1), we obtain $\omega_d = 0$, which in other words, means no Doppler effect. The problem lays on the value of

θ and the solution is not to keep the laser perpendicular to the surface of the moving strip but rather to tilted as much as possible, so that θ gets close to zero.

6.2. Functional Tests

6.2.1. Bench Test I

A typical output obtained at the bench test I is shown in figure 29.

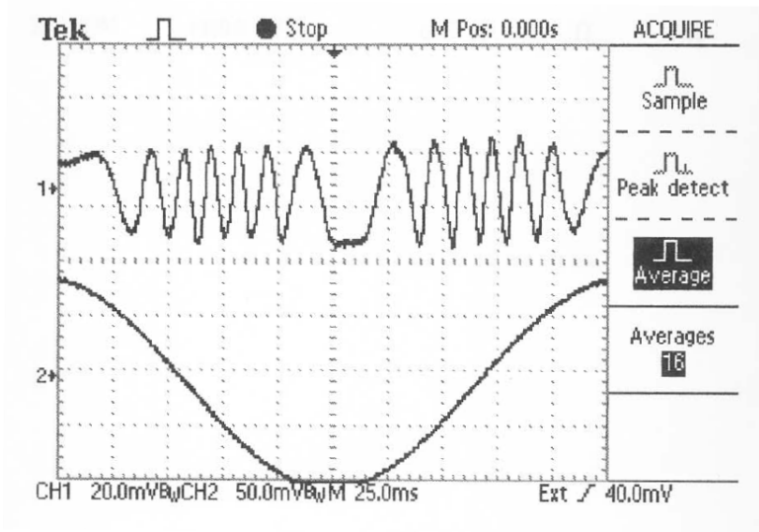


Figure 29: Typical signals observed in self-mixing – lower trace, loudspeaker membrane movement – upper trace, self-mixing signal from PD.

The lower trace in figure 29 is the signal applied to achieve the periodic target movement, and the resultant intensity modulation (upper trace) is the self-mixing interference signal observed. The extremes of the displacement curve correspond to the zero-velocity instants. During the positive velocity, or when approaching, each of the sawtooth-like waveforms rises rapidly and falls slowly, while during the negative velocity vice versa.

The spectra for the time series depicted in figure 29 are shown in figure 30. Five different modulated frequencies are shown.

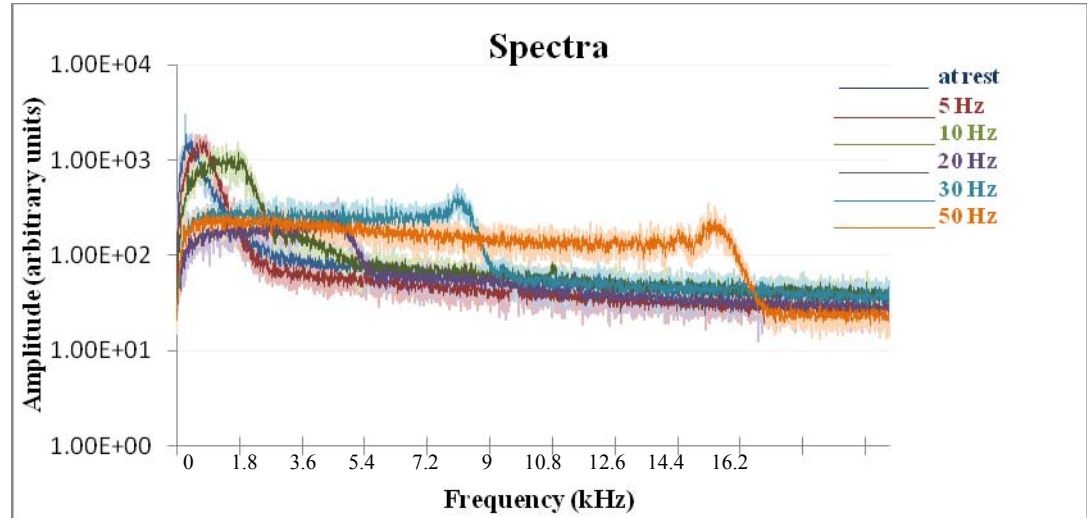


Figure 30: Frequency Beating Spectra.

We will now use these results to calculate the membrane amplitude.

If the membrane position (x) is given by $x = A\cos(\omega t)$, the velocity will be:

$$v = -A\omega\sin(\omega t)$$

Taking the modulated frequency of 50 Hz (orange line), in figure 29 where a maximum frequency of 15 kHz is readable, and for the values used in the experiment:

$$\omega_d = \frac{4\pi}{\lambda_t} \times v = \frac{4\pi}{\lambda_t} \times (-A\omega\sin(\omega t)) \Leftrightarrow$$

$$\Leftrightarrow A = -\frac{\omega_d \times \lambda_t}{4\pi \times \omega} = 15 \mu m$$

Taking the modulated frequency of 30 Hz where the maximum frequency of $7 \times 10^3 \text{ Hz}$ is readable, the amplitude is approximately 12 μm .

These amplitude values are reasonable in accordance with typical data from loudspeaker datasheets.

We can also conclude that the results of the graphic are in agreement with equation (1): the Doppler frequency shift (ω_d) increases when the modulated frequency (w) increases.

It seems possible to relate the frequency beating spectra with the PDF of the raw data. This is suggested by curves of figure 29 where the typical saddle-shaped curve shows up.

As a hint, we do not close the possibility of the exploration of the connection between the beating frequency spectrum and the PDF, for standard cases.

6.3. Another Bench Tests

An experiment in which a flow regime of known characteristics is established was setup to test the LDF instrumentation. The target was a fluid with a diluted scattered (talcum powder) flowing in a transparent tube. The idea was to approximate the target as much as possible to the blood flow in terms of flow velocity. So, we developed a hydraulic model that is schematically drawn in figure 31:

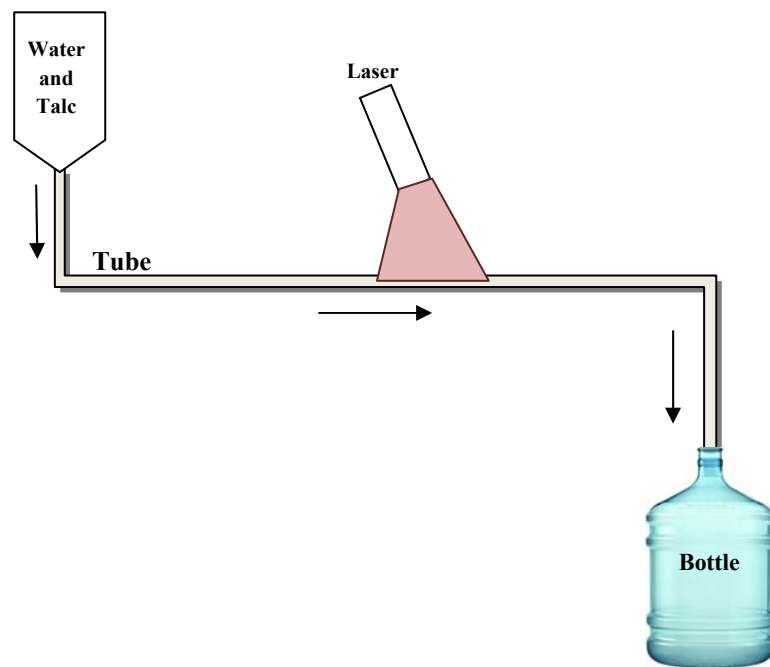


Figure 31: Hydraulic Model. The solution enters to the tube and flows through it.

The talc was chosen because it is highly scattering like the human skin. This solution was in a recipient and was then pumped through a plastic tube (inner diameter 3 mm) which was fixed in a breadboard. The different speeds of pumping of the water/talc solution were achieved by gravitation and a progressive tap. The laser Doppler fiber pigtail was positioned almost perpendicularly to the surface of the tube.

Unfortunately, there was no time to perform consistent measurements.

Another idea suggested as future work uses a peristaltic pump to obtain a pulsatile regime of similar characteristics to the human dynamic system.

7. Conclusions and Future Work

This report has reviewed the main theoretical background that underlies beneath Laser Doppler technique, as well as aspects of the detection geometries and implications derived from using optical fiber for light transportation.

The state of the art of commercially available instruments for research and clinical use has also been reviewed with a simple conclusion that equipments are very expensive and only two major European manufacturers are currently in the marketplace with interesting solutions.

Especially developed experimental set-ups have been implemented with the purpose of studying the properties of typical LDF signals. These experiments have made clear some limitations of the data acquisition hardware as well as some signal processing algorithms.

As for the data acquisition hardware, it became very clear that the NI6009 sampling rate (48 ksps total, for all channels) is not enough in many practical situations. The NI6210, with its 250 ksps, will be a better option in future developments, although it comes at a 3 times higher price.

Concerning the signal processing algorithms, it also became evident that the classic Fourier transform (or its simplified relative, the FFT) does not provide adequate information in the context of this application. In fact, for the long time intervals, that are common in LDF, the Continuous Wavelet Transform (CWT) is generally recognized as a superior analysis tool since it allows spectral analysis without loss of time information.

Experiments on the self-mixing arrangement for LDF with the loudspeaker have proved to be very effective and insightful. Data collected with this system is shown and some speculation concerning its interpretation is developed.

Data collected in this experiment is also used to determine the amplitude of the loudspeaker movement when it is driven by a sinusoidal waveform. This experiment also demonstrates the adequacy of the instrument as a laser vibrometer.

Experiments with a different scattering system – a unidirectionally moving strip of paper – were not completed, and were consequently misleading, due to lack of time.

8. References

- [1] Jones Deric P, “Medical Electro-optics: measurements in the human microcirculation”, 1987, Phys. Technol., 18, 79-85
- [2] Anderson, R.R. and Parrish, “Optical Properties of Human Skin”, 1987 (New York)
- [3] Tuchin V, “Tissue Optics: Light Scattering Methods and Instruments for Medical Diagnosis”, 2000
- [4] Fredriksson I, Fors C and Johansson J, “Laser Doppler Flowmetry – a Theoretical Framework”, 2007, Linköping University, Department of Biomedical Engineering
- [5] <http://en.wikipedia.org/>
- [6] Briers J D, “Laser Doppler, speckle and related techniques for blood perfusion mapping and imaging”, 2001, Physiol. Meas., 22, R35-R66
- [7] Forrester K R, Tutil J, Leonard C, Stewart C, Bray R C, “A Laser Speckle Imaging Technique for Measuring Tissue Perfusion”, 2004, iEEE Transactions on Biomedical Engineering, Vol. 51 No. 11, pages 2074-2084
- [8] Smedley G, Yip Kay-Pong, Wagner A, Dubovitsky S, Marsh D J, “A laser Doppler instrument for in vivo measurements of blood flow in single renal arterioles”, 1993, iEEE Transactions on Biomedical Engineering, Vol. 40 No. 3, pages 290-297
- [9] Wnag W M, Boyle J O, Grattan K T V, Palmer A W, “Self-mixing interference in a diode laser: experimental observations and theoretical analysis”, 1993, Applied Optics, vol.32 No.9, 1551-1558
- [10] Humeau A, Köitka A, Abraham P, Saumet J, L’Huillier Jean-Pierre, “Spectral components of laser Doppler Flowmetry signals recorded in healthy and type 1 diabetic subjects at rest and during a local and progressive cutaneous pressure application: scalogram analyses”, 2004, Phys. Med. Biol., 49, 3957-3970

-
- [11] Serov A, Steunacher B and Lasser T, “Full-field laser Doppler perfusion imaging and monitoring with an intelligent CMOS camera”, 2005, *Optics Express*, vol. 13 No. 17, 6416-6428
- [12] Serov A and Theo L, “Blood flow imaging is enhanced using new detector technology”, Laboratoire d’Optique Biomedicale, École Polytechnique Fédérale de Lausanne
- [13] Sinohara S, Mochizuki A, Yoshida H and Sumi M, 1986, *Appl.Opt.*, **25**, 1417–9
- [14] Slot M, KoelinkM H, Scholten F G, de Mul F F M, Weijers A L, Greve J, Graff R, Dassel A C M, Aarnoudse J G and Tuynman F H B, 1992, *Med. Biol. Eng.Comput.*, **30**, 441–6
- [15] de Mul F F M, KoelinkM H, Weijers A L, Greve J, Aarnoudse J G, Graff R and Dassel A C M, 1992, *Appl. Opt.*, **27**, 20
- [16] Jukka Hast, “Self-mixing interferometry and its applications in non invasive pulse detection”
- [17] Özdemir S K, Shinohara S, Takamiya S and Yoshida H, “Noninvasive blood flow measurement using speckle signals from a self-mixing laser diode: in vitro and in vivo experiments”, 2000, *Opt. Eng*, 39(9), 2574-2580
- [18] Petermann K, “ Laser Diode Modulation and Noise”, 1988, Kluwer Academic, Dordrecht, Netherlands
- [19] Meigas K, Hinrikus H, Kattai R, Lass J, “Self-mixing in a diode laser as a method of cardiovascular diagnostics”, January 2003, *Journal of Biomedical Optics* 8(1), 152-160
- [20] http://bmo.tnw.utwente.nl/vinay/principle_of_laser_doppler_flowm
- [21] <http://www.discovtech.com/PAGE5.htm>
- [22] http://www.perimed.se/p_Products/periflux.asp
- [23] Nilsson G E, Salerud E G, Strömberg NOT, Wårdell K, “Laser Doppler Perfusion Monitoring and Imaging”, In: Vo-Dinh T, editor: *Biomedical photonics handbook*, Boca Raton, Florida:CRC Press, 2003, p. 15:1-24
- [24] <http://sine.ni.com/nips/cds/view/p/lang/en/nid/14605>
-

[25] <http://www.mathworks.com/index.html?ref=pt>

[26] Öberg P Å, “Optical Sensors in Medical Care”, Sensors Update 3

Annex A - Simulation of the beating frequency phenomenon

%Project: 'Evaluation of Hemodynamic Parameters: LDF'
%Observation of the frequency beating phenomenon - July 2007

```
npts=50000; %number of points
na=34; %number of periods
ampl=1; %amplitude

x=seno(npts,na,ampl); % Creates a sino function

npts=50000;
na=37;
ampl=1;

y=seno(npts,na,ampl);

for k=1:npts;
    soma(k)=x(k)+y(k); %Sum of two waves
end

for t=1:npts;
    i(t)=soma(t)*soma(t); %Calculates the irradiance
end

figure(1);

subplot(4,1,1);
    plot(x);
    title('F1');

subplot(4,1,2);
    plot(y);
    title('F2');

subplot(4,1,3);
    plot(soma);
    title('Beating F1+F2');

subplot(4,1,4);
    plot(i);
    title('Irradiance');
```

Annex B - Specifications table of DTI OxyLab LDF and OxyFlo.

	Blood Perfusion	Remittance
Mode of operation	Laser-Doppler flowmetry	Intensity
No. of Channels	1 (OxyLab); 2 or 4 (OxyFlo)	1, 2 or 4
Units	0 - 9999 Blood Perfusion Units (BPU)	0 - 100% Backscatter
Range	Up to 0.35 % moving scatterers by vol.	-
Stability of Reading	1.5 % (OxyFlo); 5% (OxyLab) (motility standard)	1 %
Acquisition Time	0.09 s	1 s
Response Time	<0.1 s	1 s
Input Sampling Rate	48 kHz (16 Bit)	1 Hz (16 bit)
Output Update Rate	750 Hz	750 Hz
Output Range	0 - 5 V (1 – 9999 BPU)	0 - 5 V (0 - 100 %)
Output Resolution	0.1 BPU (60 m V)	0.002 % (60 m V)
Outputs	Analog 2 (OxyLab); 4 or 8 (OxyFlo)0	
Probe Identification	Automatic	
Flow Calibration	Factory or user. Motility standard.	
Laser Type	830±10 nm temp. stabilized semiconductor	
Laser Power	< 0.5 mW from probe	
Laser Class	Class 1 (per 21 CFR 1040 and 1040-11)	
Bandwidth	22 kHz	
Zeroing	Automatic	
Display	8-ch LED per channel (OxyFlo); 32-ch LED (OxyLab LDF)	
Dimensions	135 x 410 x 320 mm (OxyFlo); 90 x 290 x 260 (OxyLab LDF)	
Weight	3 Kg (OxyFlo); 2 Kg (OxyLab LDF)	
Power	93 – 240 VAC; 47 - 63 Hz	
Storage Temp.	5°C - 50°C	
Operating Temp.	10°C - 35°C	
Operating Humidity	0 – 70% (non condensing)	

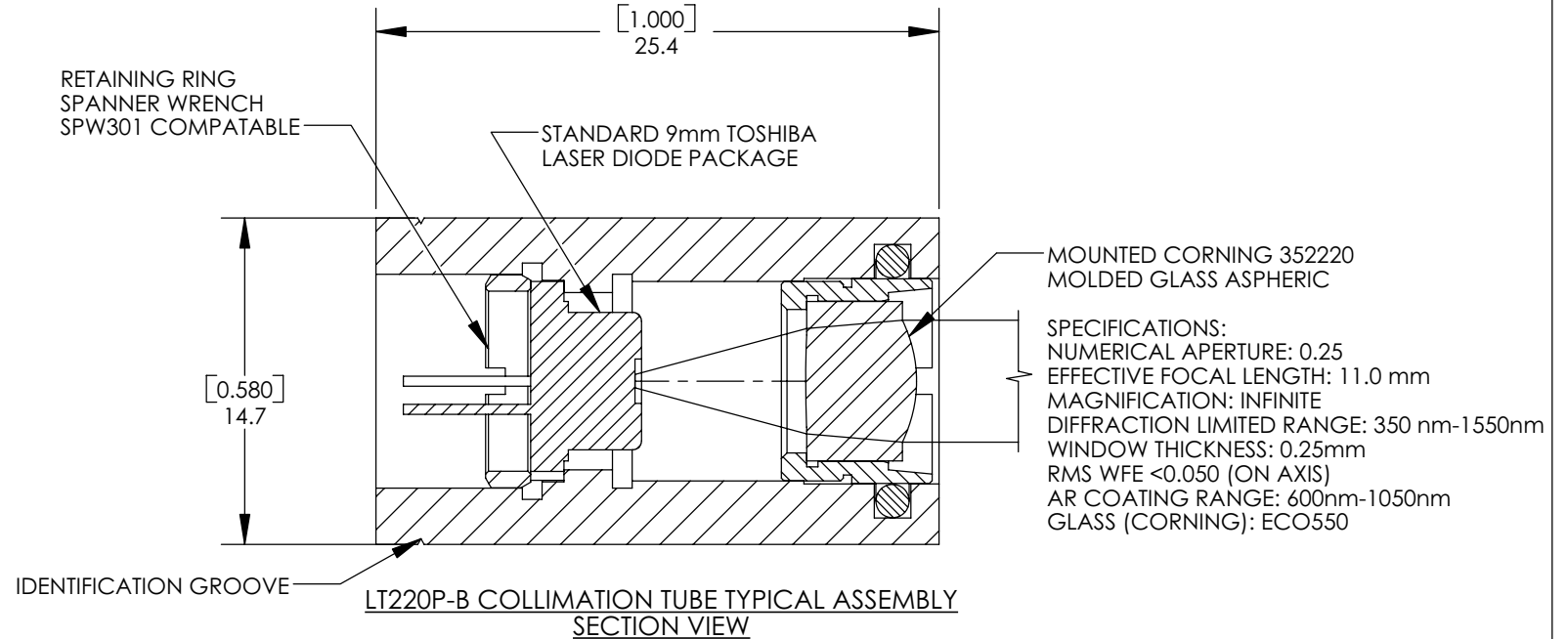
Adapted from ^[22]

Annex C - Schematics

REV. #	DESCRIPTION:	NAME/DATE:



2:1 SCALE



SPECIFICATIONS:

1. THE LT220P-B WAS DESIGNED USING THE TOSHIBA STANDARD 9mm LASER DIODE PACKAGE. THE PRINCIPLE PLANE OF THE C220TM ($f = 11\text{mm}$) IS NOMINALLY 13.47mm FROM THE LASER MOUNTING SURFACE
2. THE C220TME LENS CELL HAS $\pm 1\text{mm}$ OF ADJUSTMENT RANGE FROM THE POSITION SHOWN IN THE ASSEMBLY DRAWING
3. THE LT220A DESIGN REQUIRES THE EMITTING SURFACE OF THE LASER TO BE BETWEEN 1.7mm TO 3.2mm FROM THE $\phi 9\text{mm}$ MOUNTING FLANGE OF THE LASER

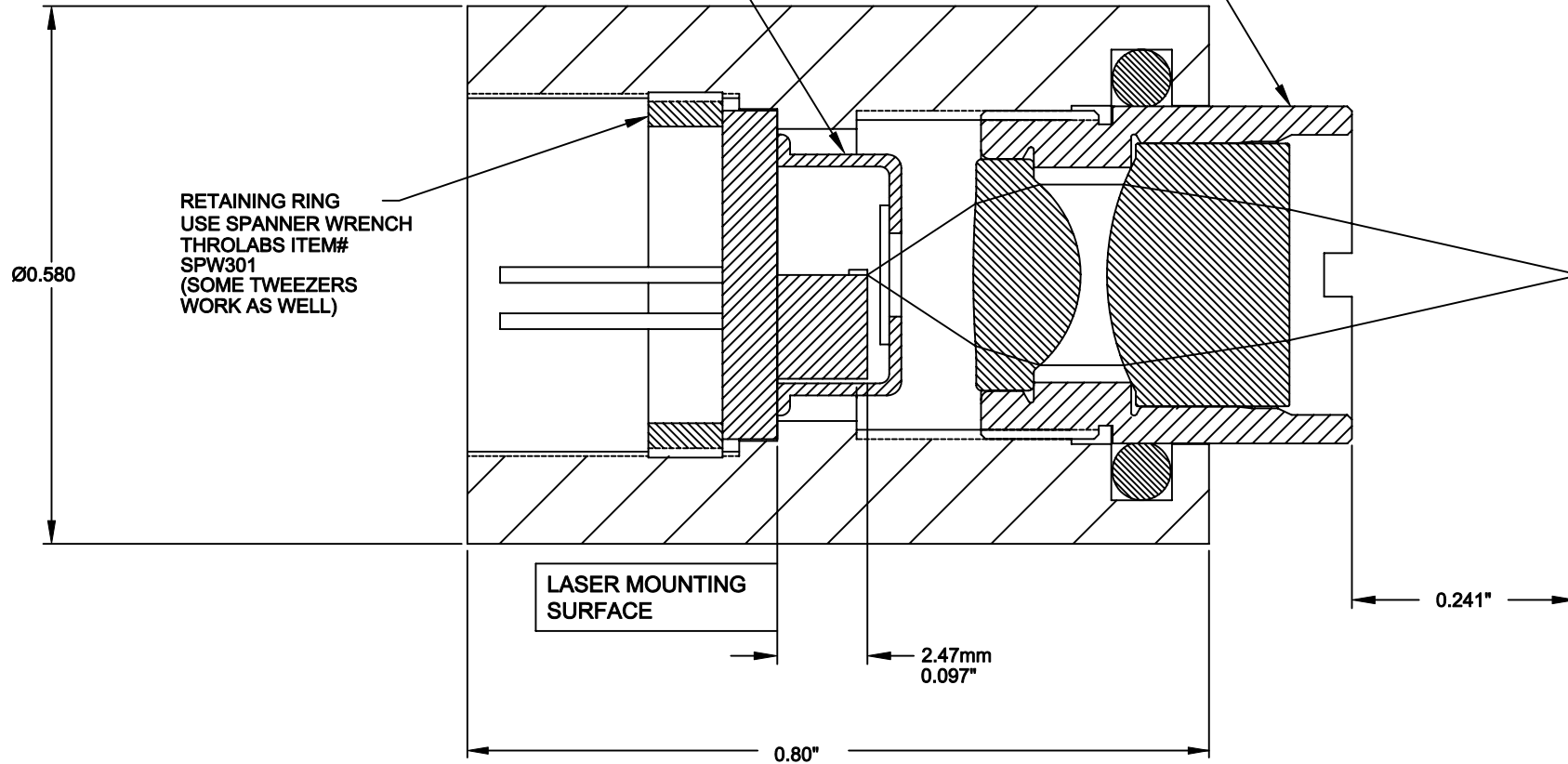
THIS DRAWING IS FOR INFORMATION ONLY
NOT INTENDED FOR MANUFACTURING

TOLERANCES	NAME	DATE
UNLESS OTHERWISE SPECIFIED:	DRAWN BAG	10/23/2006
DIMENSIONS ARE IN MILLIMETERS	ENG APPR. TO	10/23/2006
LINEAR TOLERANCES:	MFG APPR. TO	10/23/2006
ONE PLACE DECIMAL: ± 0.2	PROPRIETARY AND CONFIDENTIAL	
TWO PLACE DECIMAL: ± 0.04	THE INFORMATION CONTAINED IN THIS	
ANGULAR: $\pm 30'$	DRAWING IS THE SOLE PROPERTY OF	
	THORLABS, INC. ANY REPRODUCTION	
	IN PART OR AS A WHOLE WITHOUT	
	THE WRITTEN PERMISSION OF	
	THORLABS, INC. IS PROHIBITED.	

THORLABS INC. PO BOX 366 NEWTON NJ			
TITLE: LT220P-B COLLIMATION			
MATERIAL: N/A			SIZE A
SCALE: 3:1		REV. SHEET 1 OF 1	
DWG. NO. 0895-E01		PART NO. LT220P-B	

TOSHIBA DIODE LASER
STANDARD 9mm PACKAGE

Annex C - Schematic S230220P



LT230220P-B FOCUSING TUBE ASSEMBLY

SECTION VIEW

INFORMATION ONLY, NOT FOR MANUFACTURING

CORNING 350230 MOLDED GLASS ASPHERIC LENS
 NUMERICAL APERTURE: 0.55
 EFFECTIVE FOCAL LENGTH: 4.5mm
 MAGNIFICATION: INIFINITE
 DIFFRACTION LIMITED RANGE: 600nm - 1550nm
 WINDOW THICKNESS: 0.250mm BK7/1.51
 RMS WFE <0.050 (on axis)
 AR COATING RANGE: 600nm - 1050nm

CORNING 350220 MOLDED GLASS ASPHERIC LENS
 NUMERICAL APERTURE: 0.25
 EFFECTIVE FOCAL LENGTH: 11.0mm
 MAGNIFICATION: INIFINITE
 DIFFRACTION LIMITED RANGE: 350nm - 1550nm
 WINDOW THICKNESS: 0.250mm BK7/1.51
 RMS WFE <0.050 (on axis)
 AR COATING RANGE: 600nm - 1050nm

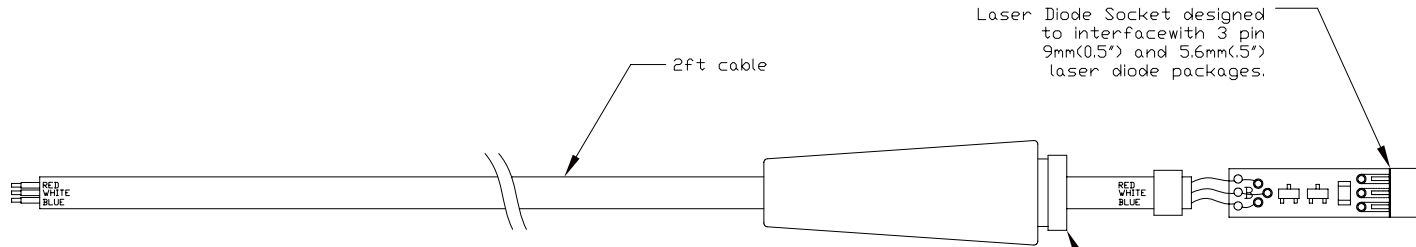
THORLABS				PO BOX 366 NEWTON NJ	
TITLE 9mm LASER TUBE WITH C230220P CELL					
TOL: X:XXX=+/-0.003 ANGULAR +/-30'					
MATERIAL NA				WHERE USED	
DRAWN GM	ENGR. JJT	APPROVED		WEB MECHANICAL DRAWING	
DATE 01/07/99	REV A	SIZE C	SHEET 1 OF 1		
DWG NO. 1607-E0W		PART NO. LT230220P-B			

Annex C - Schematics

Laser Driver Wire Connections

Color	Laser Diode Pin Conf.
Red	Photodiode Anode (PDA)
White	Photodiode Cathode,
	Laser Diode Anode (PDK, LDA)
Blue	Laser Diode Cathode (LDK)

Caution:
The SR9A should only
be used for the laser
diode pinout provided below



Note:

The SR9 strain reliefs are designed for laser diodes with voltage drops of less than 3.3V.

A 3.3V Zener diode and a Schotky diode are provided for extra ESD protection. Anti static precautions should still be used to prevent damage to the laser diode.

13/32"-40 THREAD
Designed to mate
with Thorlabs LT
series colimating
tubes.

LASER DIODE
PINOUT



SOCKET
FRONT VIEW



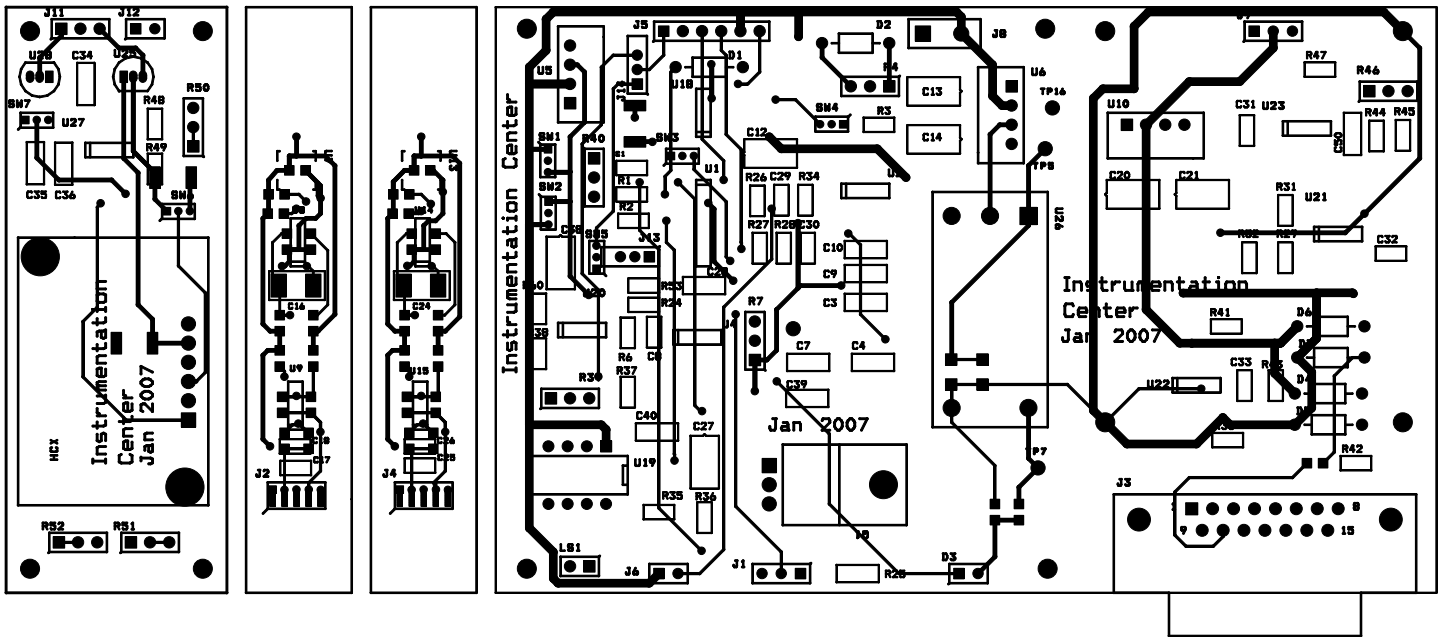
DIODE PINOUT
TOP VIEW



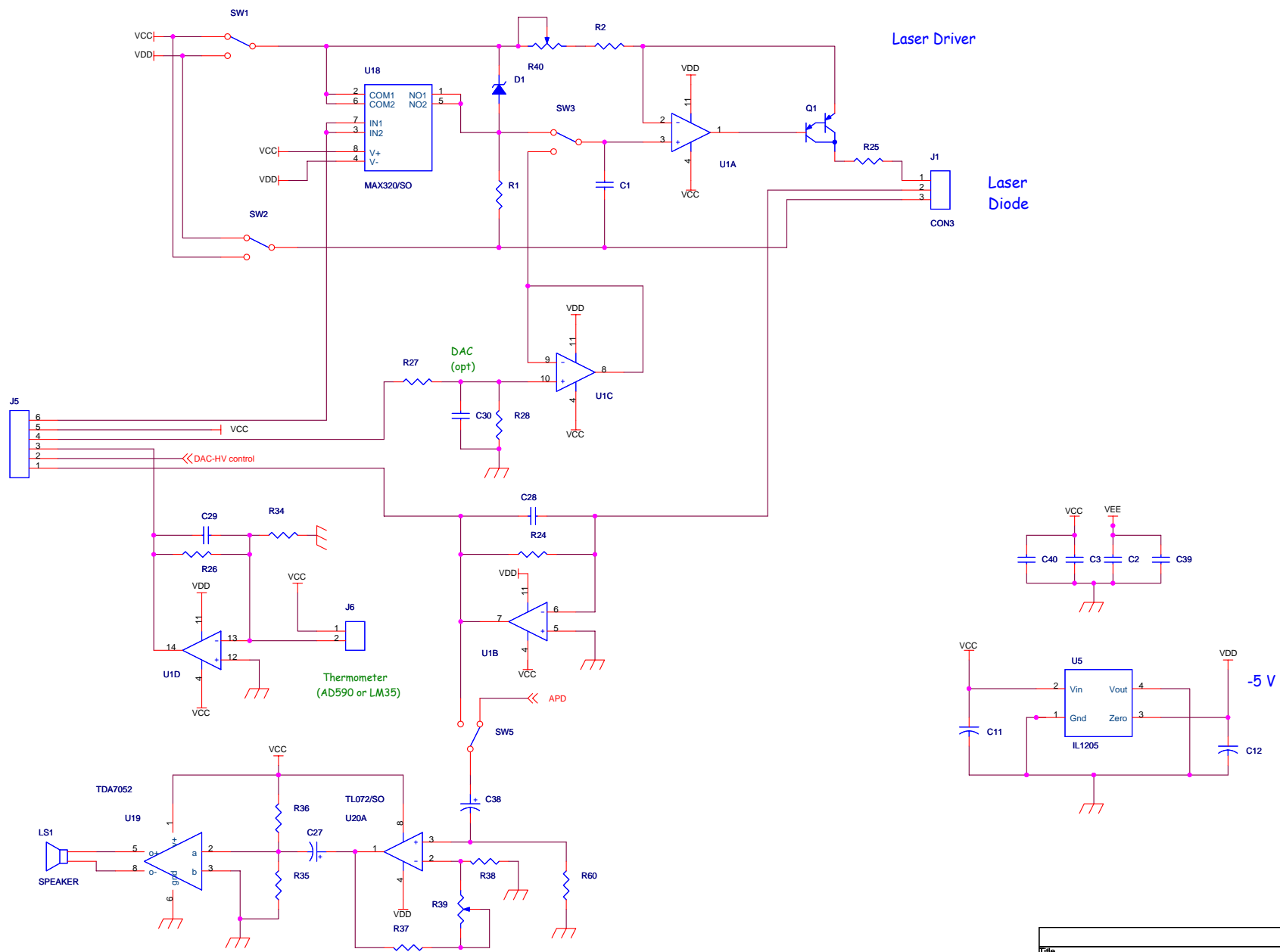
INFORMATION ONLY, NOT FOR MANUFACTURING

THORLABS <small>INC</small>				PO BOX 366 NEWTON NJ	
TITLE: STYLE A STRAIN RELIEF					
TOL: X.XXX=+/-0.005 X.XX=+/-0.010 ANGULAR +/-30'					
SURF. FINISH: 32 MICROINCHES UNLESS OTHERWISE NOTED					
DRAWN	ENGINEER	APPROVED			
EC	EC	EC		EC	
MATERIAL: SR9A					
DATE	REV	SIZE	SHEET	DRAWING SCALE	
3/26/03	B	A	1 OF 1	1" = 1"	
DWG NO.			PART NO.		
2195-E01			SR9A		

Annex D - PCB design



Annex E - Schematic of the Laser Driver



Title		
Laser Driver / Amp		
Size	Document Number	Rev
A3	<Doc>	2
Date:	Thursday, November 30, 2006	Sheet 3 of 3

Annex E - Schematic of the Laser Driver

Annex F - Specifications of the Low-Cost Multifunction DAQ for USB

Low-Cost Multifunction DAQ for USB

Specifications

Typical at 25 °C unless otherwise noted.

Analog Input

Absolute accuracy, single-ended

Range	Typical at 25 °C (mV)	Maximum (0 to 55 °C) (mV)
±10	14.7	138

Absolute accuracy at full scale, differential¹

Range	Typical at 25 °C (mV)	Maximum (0 to 55 °C) (mV)
±20	14.7	138
±10	7.73	84.8
±5	4.28	58.4
±4	3.59	53.1
±2.5	2.56	45.1
±2	2.21	42.5
±1.25	1.70	38.9
±1	1.53	37.5

Number of channels..... 8 single-ended/4 differential
 Type of ADC Successive approximation

ADC resolution (bits)

Module	Differential	Single-Ended
USB-6008	12	11
USB-6009	14	13

Maximum sampling rate (system dependent)

Module	Maximum Sampling Rate (kS/s)
USB-6008	10
USB-6009	48

Input range, single-ended ±10 V
 Input range, differential ±20, ±10, ±5, ±4, ±2.5, ±2, ±1.25, ±1 V
 Maximum working voltage ±10 V
 Overvoltage protection ±35 V
 FIFO buffer size 512 B
 Timing resolution 41.67 ns (24 MHz timebase)
 Timing accuracy 100 ppm of actual sample rate
 Input impedance 144 k
 Trigger source..... Software or external digital trigger
 System noise..... 0.3 LSB_{rms} (±10 V range)

Analog Output

Absolute accuracy (no load) 7 mV typical, 36.4 mV maximum at full scale
 Number of channels..... 2
 Type of DAC Successive approximation
 DAC resolution..... 12 bits
 Maximum update rate 150 Hz, software-timed

Output range 0 to +5 V
 Output impedance..... 50 Ω
 Output current drive 5 mA
 Power-on state..... 0 V
 Slew rate..... 1 V/μs
 Short-circuit current 50 mA

Digital I/O

Number of channels..... 12 total
 8 (P0.<0..7>)
 4 (P1.<0..3>)
 Direction control Each channel individually programmable as input or output
 Output driver type
 USB-6008 Open-drain
 USB-6009 Each channel individually programmable as push-pull or open-drain
 Compatibility CMOS, TTL, LVTTTL
 Internal pull-up resistor 4.7 kΩ to +5 V
 Power-on state..... Input (high impedance)
 Absolute maximum voltage range..... -0.5 to +5.8 V

Digital logic levels

Level	Min	Max	Units
Input low voltage	-0.3	0.8	V
Input high voltage	2.0	5.8	V
Input leakage current	-	50	μA
Output low voltage (I = 8.5 mA)	-	0.8	V
Output high voltage (push-pull, I = -8.5 mA)	2.0	3.5	V
Output high voltage (open-drain, I = -0.6 mA, nominal)	2.0	5.0	V
Output high voltage (open-drain, I = -8.5 mA, with external pull-up resistor)	2.0	-	V

Counter

Number of counters 1
 Resolution 32 bits
 Counter measurements..... Edge counting (falling edge)
 Pull-up resistor..... 4.7 kΩ to 5 V
 Maximum input frequency 5 MHz
 Minimum high pulse width..... 100 ns
 Minimum low pulse width..... 100 ns
 Input high voltage 2.0 V
 Input low voltage 0.8 V

Power available at I/O connector

+5 V output (200 mA maximum) +5 V typical
 +4.85 V minimum
 +2.5 V output (1 mA maximum) +2.5 V typical
 +2.5 V output accuracy 0.25% max
 Voltage reference temperature drift... 50 ppm/°C max

¹Input voltages may not exceed the working voltage range.

Annex G – Matlab program to observe LDF data acquisition

```
% Project: 'Evaluation of Hemodynamic Parameters: LDF'  
% Observation of the LDF data acquisition  
%  
  
    st=2.5e-5;  
    f1=1;  
    f2=20000;  
  
[filename,path] = uigetfile('*.txt','Choose a file');  
  
x= load(filename);  
npts=length(x)  
  
a = x(:,1);  
  
clear x;  
  
[A,B]=max(abs(a));  
  
ascale=linspace(0,(npts-1)*st,npts);  
length(ascale);  
  
figure(1)  
    plot(ascale,a,'b')      , axis([0, npts*st, 0, A])  
    title(['LDF      npts = ',num2str(npts)])  
  
figure(2)  
    plot(ascale,a,'b')      , axis([1, 1.2, 0, A])  
    title(['LDF      npts = ',num2str(npts)])  
  
fa=BandPassFilter(a, npts, st, f1, f2);  
  
[A,B]=max(abs(fa));  
  
t1=0.1;  
t2=0.14;  
  
figure(3)  
    plot(ascale,-1*fa,'b')  , axis([t1, t2, -A, A])  
    title(['LDF      npts = ',num2str((t2-t1)/st)])  
  
y=fftshift(fft(a));  
  
y(npts/2+1)=0;  
  
[A,B]=max(abs(y));
```

```

fscale=linspace(-0.5/st, 0.5/st, npts);

figure(4)
plot(fscale, abs(y))      , axis([0, 0.5/st, 0, A ])

title(['FFT' ])

m=20;
nnn=round(npts/2/m);

for w=1:nnn
    sum=0;
    for k=1:10
        sum=sum+abs(y(k+w*m));
    end
    fg(nnn-w+1)=sum;
end

%   n2=length(fg);
%
%   f2scale=linspace(0, 0.5/st, n2);
%   figure(5)
%       plot(f2scale,fg)
%
s=fg.';
sc=f2scale.';

save('res_50_10.txt', 's', '-ASCII');
save('res_50_10_sc.txt', 'sc', '-ASCII');

clear all

```